

# Water Resources Research®



## RESEARCH ARTICLE

10.1029/2023WR036394

### Special section

Forcing, response, and impacts of coastal storms in a changing climate

## Saltwater Intrusion Into a Confined Island Aquifer Driven by Erosion, Changing Recharge, Sea-Level Rise, and Coastal Flooding

S. Stanic<sup>1</sup>, N. K. LeRoux<sup>1</sup> , A. Paldor<sup>2</sup> , A. A. Mohammed<sup>1,3,4</sup> , H. A. Michael<sup>2,5</sup> , and B. L. Kurylyk<sup>1</sup> 

### Key Points:

- A surface-subsurface numerical model is used to investigate climate change impacts on island groundwater resources used for water supply
- The confined aquifer is resilient to storm surges which only salinize the unpumped surficial aquifer before being flushed
- Coastal erosion and recharge reductions result in the most saltwater intrusion and can work in tandem to threaten future water supply

### Supporting Information:

Supporting Information may be found in the online version of this article.

### Correspondence to:

B. L. Kurylyk,  
[barret.kurylyk@dal.ca](mailto:barret.kurylyk@dal.ca)

### Citation:

Stanic, S., LeRoux, N. K., Paldor, A., Mohammed, A. A., Michael, H. A., & Kurylyk, B. L. (2024). Saltwater intrusion into a confined island aquifer driven by erosion, changing recharge, sea-level rise, and coastal flooding. *Water Resources Research*, 60, e2023WR036394. <https://doi.org/10.1029/2023WR036394>Received 29 SEP 2023  
Accepted 16 DEC 2023

<sup>1</sup>Department of Civil and Resource Engineering and Center for Water Resources Studies, Dalhousie University, Halifax, NS, Canada, <sup>2</sup>Department of Earth Sciences, University of Delaware, Newark, DE, USA, <sup>3</sup>Department of Earth and Environmental Sciences, Syracuse University, New York, NY, USA, <sup>4</sup>Department of Civil and Environmental Engineering, Syracuse University, Syracuse, NY, USA, <sup>5</sup>Department of Civil and Environmental Engineering, University of Delaware, Newark, DE, USA

**Abstract** Aquifers on small islands are at risk of salinization due to low elevations and limited adaptive capacity, and present risks will be exacerbated by climate change. Most studies addressing small-island saltwater intrusion (SWI) have focused on homogeneous sandy islands and one or two hydraulic disturbances. We herein investigate SWI dynamics in a layered, confined island aquifer in response to multiple environmental perturbations related to climate change, with two considered in tandem. Our field and modeling work is based on an island aquifer that provides the drinking water supply for an Indigenous community in Atlantic Canada. Observation well data and electrical resistivity profiles were used to calibrate a numerical model (HydroGeoSphere) of coupled groundwater flow and salt transport. The calibrated model was used to simulate the impacts of climate change including sea-level rise (SLR), storm surge overtopping, changing aquifer recharge, and erosion. Simulated aquifer conditions were resilient to surges because the confining layer prevented deeper saltwater leaching. However, reduced recharge and erosion resulted in saltwater wedge migration of 170 and 110 m, respectively when considered individually, and up to 295 m (i.e., into the wellfield) when considered together. Despite the confining conditions, SLR resulted in wedge migration up to 55 m as the confining pressures were not sufficient to resist wedge movement. This is the first study to harness an integrated, surface-subsurface hydrologic model to assess effects of coastal erosion and other hydroclimatic stressors on island aquifers, highlighting that climate change can drive extensive salinization of critical groundwater resources.

**Plain Language Summary** Due to their limited resources and adaptive capacity, small islands are highly vulnerable to climate change impacts, including saltwater intrusion. Freshwater needs on small islands are often sourced from small aquifers that are in delicate balance between conditions in the ocean, atmosphere, and land. In this study, we investigate the movement of saltwater into the freshwater aquifer of a small island that provides drinking water resources for an Indigenous First Nation. We consider climatic changes in the ocean (sea-level rise (SLR), storm surges, and related coastal erosion) and atmosphere (changes to net precipitation) and associated impacts to the island's fresh groundwater resources. We use field data paired with a mathematical model and demonstrate that the pressurized conditions of the layered island aquifer make it more resilient to SLR than unconfined aquifers in sandy islands are. However, the aquifer's freshwater volume is susceptible to coastal erosion and reduced precipitation, particularly when these happen at the same time. Results point to coastal erosion as a potential widespread driver of freshwater loss along eroding portions of the global coastline.

## 1. Introduction

Coastal zones worldwide are densely populated and rely heavily on groundwater resources to meet their industrial and domestic water demands (Barlow & Reichard, 2010; Kundzewicz et al., 2007; Michael et al., 2017). In particular, islands are home to over 700 million people worldwide (World Population Review, 2023), with almost half of island nations in a state of water stress given their dependence on vulnerable groundwater resources for drinking water (Holding et al., 2016). The reliance of small-island populations on groundwater resources is often due to the limited availability of fresh surface water resources (Gohar et al., 2019; Tribble, 2008; White &

© 2024 The Authors.

This is an open access article under the terms of the [Creative Commons Attribution-NonCommercial License](https://creativecommons.org/licenses/by-nc/4.0/), which permits use, distribution and reproduction in any medium, provided the original work is properly cited and is not used for commercial purposes.

Falkland, 2010); however, the groundwater resources (freshwater lenses) on small islands are also precarious due in part to the limited area available for fresh recharge (Briggs et al., 2021; Volker et al., 1985). In general, the proximity to the coast, low surface elevations, and low hydraulic inertia (low volumes) of small-island aquifers paired with the high groundwater dependence in these settings make island freshwater resources highly sensitive to hydroclimatic changes and groundwater pumping (Cantelon et al., 2022; Oppenheimer et al., 2019; Werner et al., 2013, 2017).

Saltwater intrusion (SWI) research in coastal aquifers has predominantly focused on lateral SWI, which is defined as the landward migration of the subsurface saltwater wedge due to land-ocean hydraulic gradient changes caused by sea-level rise (SLR), pumping, or reduced recharge (Ketabchi et al., 2016; Werner et al., 2013). Studies have generally found that “recharge-limited” aquifers that are able to maintain the hydraulic gradient under SLR experience less SWI than “topography-limited” aquifers that are unable to maintain the gradient (Carretero et al., 2013; Michael et al., 2013; Werner & Simmons, 2009). Factors such as the extent of surface inundation due to SLR, the seaward groundwater flux, groundwater recharge, and aquifer storage control the rate and pattern of freshwater-saltwater interface migration (Ataie-Ashtiani et al., 2013; Ketabchi et al., 2016; Morgan & Werner, 2014).

Until recently, vertical SWI driven by infiltration of flooded seawater following coastal storms had received less attention than SWI driven by SLR (Cantelon et al., 2022). However, recent studies have shown that vertical SWI dynamics in response to coastal flooding depend on many factors including geology, spatiotemporal extent of flooding, inundation frequency, and topography (e.g., LeRoux et al., 2023; Tackley et al., 2023; Vithanage et al., 2012; Yu et al., 2016). Given that changes in coastal storm intensity and frequency are expected to occur with a warmer ocean (Greenan et al., 2019; IPCC, 2021), vertical SWI caused by flooding may occur with shorter return periods that do not provide enough time for aquifer recovery between storms (Paldor & Michael, 2021). Groundwater recharge can also influence both lateral and vertical SWI dynamics as reduced recharge can draw the freshwater-saltwater interface landward and retard aquifer freshening following vertical SWI (Chang & Clement, 2012; Chui & Terry, 2013; Holding & Allen, 2015a).

Relatively recent field studies have considered the importance of coastal erosion as a SWI driver (e.g., Cantelon et al., 2023; Schneider & Kruse, 2003). Also, a limited number of analytical or numerical modeling investigations have investigated the impacts of erosion on island groundwater resources and concluded that erosion can drive SWI, in part due to a reduction in the area available for fresh recharge (Chesnaux et al., 2021; Lemieux et al., 2015; Schneider & Kruse, 2006). Morphologic change occurs in tandem with other climate change stressors, which causes erosion, SLR, and storm surge inundation to interact with one another (Bilskie et al., 2014; Walther et al., 2017) and influence vertical SWI patterns (Cantelon et al., 2022, 2023). In addition to reducing the area available for fresh recharge, changes in the coastline morphology, including slope, affect surface and subsurface flow patterns (Passeri et al., 2015; Volker et al., 1985; Zhang et al., 2016) and potentially wave runup and water table overheight (Kang et al., 1994; Nielsen & Hanslow, 1991). Also, the influence of aquifer confining conditions on the response to SLR and other forcings is relatively unstudied compared to the dynamics of homogeneous, unconfined aquifers, such as those along sandy beaches. In general, hydraulic conductivity distributions can strongly influence the response of an aquifer to SWI drivers (Holding & Allen, 2015b; Ketabchi et al., 2014; Paldor et al., 2019; Vithanage et al., 2012).

The present study's goal is to investigate impacts of different atmospheric and oceanic climate change stressors on small-island groundwater resources. Specifically, we use a calibrated, numerical surface-subsurface flow and transport model to simulate the impacts of SLR, storm surge overtopping, changing recharge, and coastal erosion on fresh groundwater resources in a two-layered, confined, island aquifer. Our approach is novel as this is the first integrated hydrologic modeling study of the impacts of coastal erosion and other hydroclimatic stressors on SWI along island or continental coastlines. Past related work has considered the impacts of one erosion scenario on barrier island freshwater resources in models restricted to the subsurface (Lemieux et al., 2015; Schneider & Kruse, 2006) or the effects of SWI from coastal flooding on idealized (e.g., Holding & Allen, 2015b) or atoll (Storlazzi et al., 2018) islands. Herein, a coupled, integrated surface and subsurface flow and transport model is applied to study SWI dynamics in response to different erosional and hydrodynamic stressors, with the two “worst-case” perturbations modeled in tandem to investigate compounding effects. Most previous island groundwater models have considered sandy, barrier island aquifers rather than confined (layered) bedrock aquifers like in the present study, but layered island aquifers are ubiquitous worldwide (Falkland, 1993; Robins &

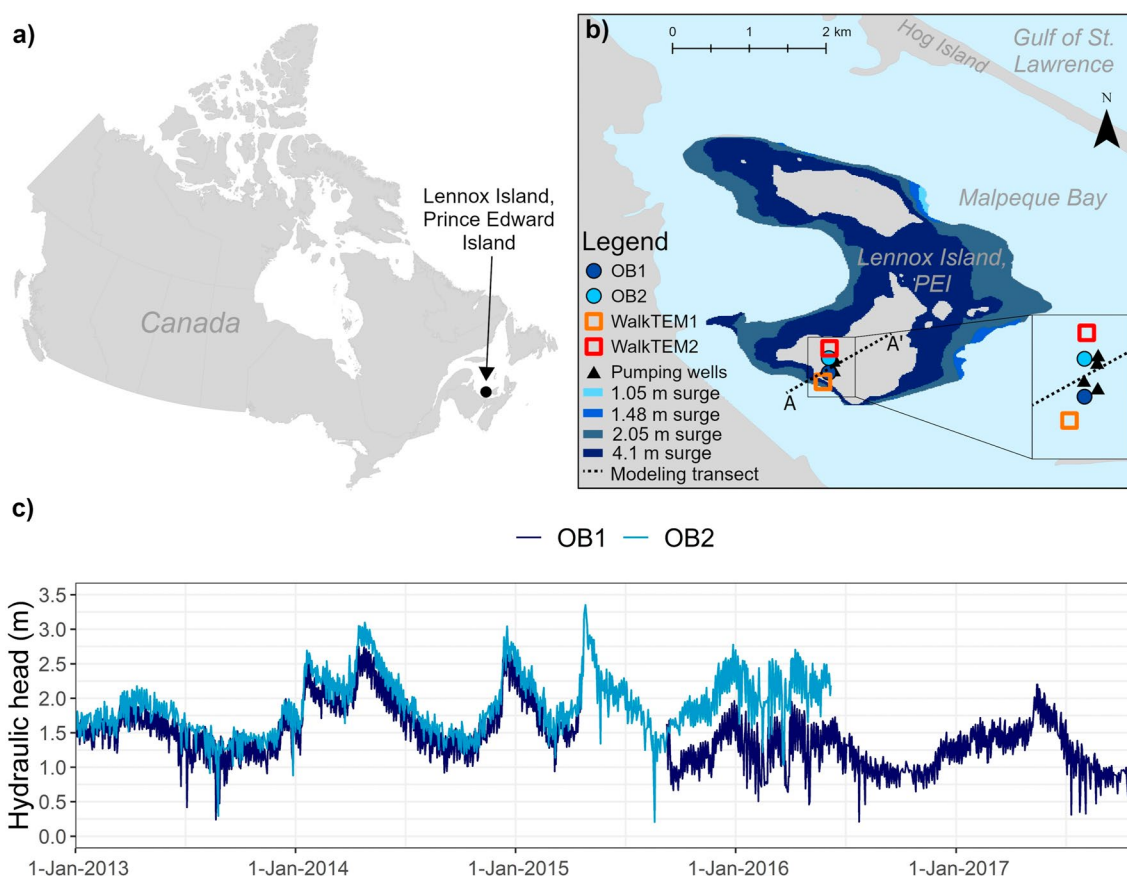


**Figure 1.** Maps of study site: (a) Prince Edward Island (PEI), Canada, with the location of Lennox Island noted by black dot; (b) Lennox Island and nearby barrier island Hog Island in Malpeque Bay. The flood extents for surge simulations described in Table 2 (Section 2.4) are shown (underlying gray layer is entire island), and locations of pumping wells, observation wells, and geophysical measurement locations are noted in the transparent inset. (c) Groundwater head fluctuations in observation wells OB1 and OB2 from 2013 to 2017 (see panel b for locations and colors, data from Public Services and Procurement Canada, pers. comm. 2020).

Lawrence, 2000; UNESCO-IHP & UNEP, 2016; Vacher & Quinn, 1997). The field work and associated numerical modeling for this project was conducted on Lennox Island (Prince Edward Island, Canada), in partnership with the Lennox Island Mi'kmaq First Nation and the Mi'kmaq Confederacy of Prince Edward Island. Hydrogeological studies that combine numerical modeling with field data are critical to understand the important factors that influence vulnerable island aquifers in the face of present and future oceanic and atmospheric climate change.

## 2. Materials and Methods

### 2.1. Study Site

Lennox Island is a small (5.02 km<sup>2</sup>) island off the northern shore of the Canadian province of Prince Edward Island (Figure 1). Lennox Island is protected from the high wave energy of the Gulf of St. Lawrence by the Hog Island (Mi'kmaq, Pituamkek) barrier chain that attenuates wave action in Malpeque Bay (Figure 1). Lennox Island is home to the Lennox Island Mi'kmaq First Nation which has approximately 450 residents. Despite its location in the sheltered Malpeque Bay, Lennox Island's soft sandstone coastline can erode up to 90 cm yr<sup>-1</sup>, with pronounced erosion during storm events (MacDonald, 2014; Majeed, 2015). The island has an average topographic slope of approximately 0.4%, with the highest elevation approximately 8 m above sea level. Like most of the north shore of Prince Edward Island, tides around Lennox Island are mixed, mostly semi-diurnal, with a typical range of ~1 m (Armon & McCann, 1979).

The geology of Lennox Island is typical of much of Prince Edward Island and is part of the Kildare Capes Formation, a series of upward-fining red bed sandstones with intraformational mudstones (van de Poll, 1989). The upper portion of the sandstone deposits contains a dense fracture network, mainly oriented along the bedding planes (Jiang et al., 2004), in which groundwater flow is concentrated. However, vertical/sub-vertical fractures

can also allow rapid water infiltration deeper into Prince Edward Island bedrock (Carr, 1969). The heterogeneous and fractured geology of Prince Edward Island can result in complex aquifer-ocean interactions with multiple salt wedges at depth (van der Kamp, 1981), focused submarine groundwater discharge via intertidal springs (KarisAllen et al., 2022), and complex contaminant transport dynamics (Pavlovskii et al., 2023). However, past groundwater modeling work on Prince Edward Island has employed an equivalent porous medium approach (e.g., Jiang & Somers, 2009). On Lennox Island, a deeper confined fractured sandstone/mudstone aquifer is separated from the surficial till aquifer by a confining unit consisting of low-permeability mudstone. Four production wells installed in the deep, confined aquifer on Lennox Island (Jacques Whitford, 2007) are pumped on a rotational basis and provide the First Nation's water supply (triangles, Figure 1b). Extraction rates were monitored between 2010 and 2018, with an average island-wide pumping rate of  $130 \text{ m}^3 \text{ day}^{-1}$  (PSPC, 2018).

Prince Edward Island receives on average  $1,100 \text{ mm yr}^{-1}$  of precipitation based on data from climate stations at Harrington and Summerside and previous island-wide studies (ECCC, 2020a, 2020b; Jiang et al., 2004), with  $\sim 30\text{--}40\%$  of precipitation recharging aquifers (Jiang et al., 2004; Jiang & Somers, 2009; Zebarth et al., 2015). The groundwater elevation on Prince Edward Island displays a bimodal fluctuation annually, with the highest levels occurring in spring and fall, and the lowest during late summer and in winter months when precipitation is stored in the snowpack (Jiang & Somers, 2009; PSPC, 2018). Several studies have performed hydrologic balances for Prince Edward Island watersheds, resulting in calculated evapotranspiration rates ranging from  $382$  to  $730 \text{ mm yr}^{-1}$  and runoff ranging from  $101$  to  $209 \text{ mm yr}^{-1}$  (Afzaal et al., 2020; De Jong et al., 2008; Paradis et al., 2016; Vigneault et al., 2007).

## 2.2. Field Methods and Data Sources

Data for two observation wells (OB1 and OB2, Figures 1b and 1c) in the lower aquifer on the island were shared by the Lennox Island First Nation via Public Services and Procurement Canada for 2013–2017. The average hydraulic heads for OB1 and OB2 are  $1.44$  and  $1.83 \text{ m}$  above sea level, respectively (Figure 1c), with an average horizontal hydraulic gradient between the wells of about  $0.002$ . Hydraulic head maxima occur around late December/early January, and April or May, generally coinciding with late-fall precipitation and spring snowmelt, respectively.

To estimate the freshwater-saltwater interface location, time-domain electromagnetic geophysical measurements with a WalkTEM (ABEM) were used to determine the bulk ground resistivity at the shoreline and a more inland location close to the wellfield (Figure 1b). This system has been successfully used to map fresh and saline groundwater zones in other studies of small-island aquifers (e.g., Briggs et al., 2021; Cantelon et al., 2023). Twenty-meter transmitter loops were used for each location with measurements collected using the  $10 \text{ ms}$ , dual moment current configuration, with at least 5 stacks per station and 39 gates per pulse. The raw resistivity data were inverted using the Aarhus SPIA software (SPIA, 2020) to produce 1D resistivity profiles. A modified version of Archie's Law for saturated medium (Glover, 2016; Winsauer & Shearin, 1952, and Text S2 in Supporting Information S1) was used to calculate the porewater electrical conductivity from the bulk ground resistivity produced by the WalkTEM measurement inversion. To parameterize this form of Archie's Law, values from Hill and Milburn (1956) for a shaly sandstone with chiefly quartz cementation were used for the cementation exponent ( $1.65$ ) and tortuosity ( $1.7$ ).

Climate data for Lennox Island were obtained from the NASA Prediction of Worldwide Energy Resources (POWER) Reanalysis tool (NASA POWER Project, 2022), which provided data for a grid cell (global  $1^\circ$  latitude/longitude) including Lennox Island, along with dewpoint temperature and relative humidity from August until the end of December 2021. An average potential evapotranspiration rate of  $588 \text{ mm yr}^{-1}$  and an average precipitation rate of  $1,100 \text{ mm yr}^{-1}$  were calculated from the 2013–2017 NASA Power Reanalysis data set. This yielded a recharge (precipitation minus potential evapotranspiration) of  $512 \text{ mm yr}^{-1}$ , in line with other hydrogeological studies on Prince Edward Island (Jiang et al., 2004; Jiang & Somers, 2009). Further details on recharge estimation for this study, including evaporation calculations and a comparison of local climate data with the NASA POWER Reanalysis tool, is provided Text S1 in Supporting Information S1.

## 2.3. Numerical Modeling Methods

HydroGeoSphere (Aquanty Inc, 2015) is a numerical model that fully couples variable-density surface and subsurface flow, along with solute transport, allowing for exchange between surface and subsurface domains. Given the storm surge overtopping scenarios described later, this capacity to simulate coupled surface and subsurface flow and transport was the primary reason for selecting this model. HydroGeoSphere uses the finite

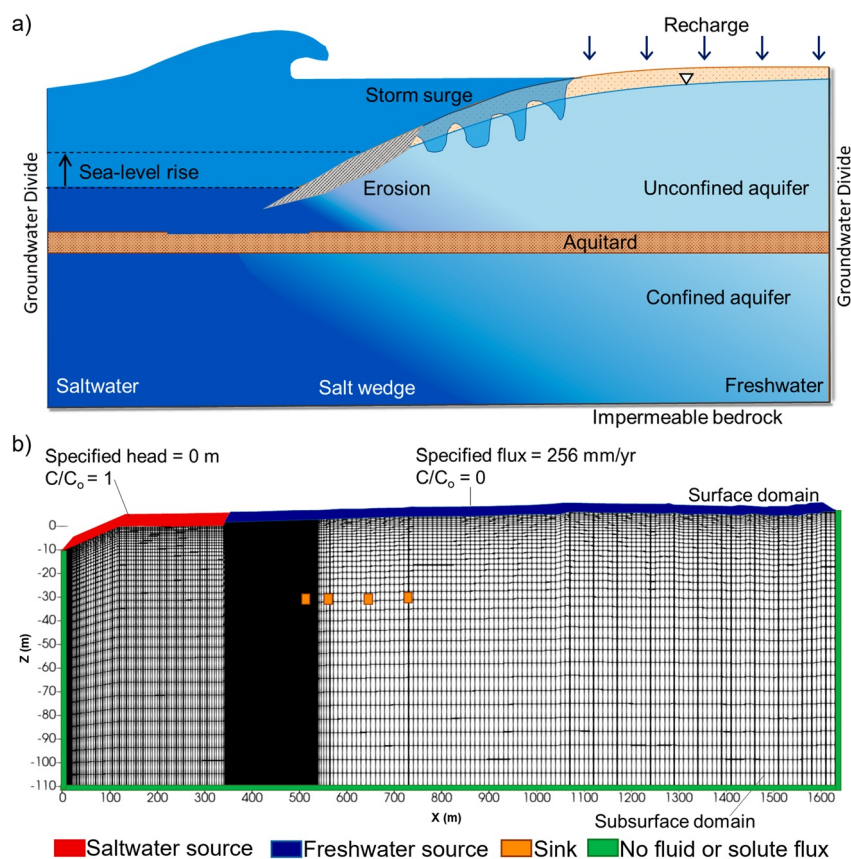


**Figure 2.** (a) Conceptual diagram of the chosen cross-section on Lennox Island (see transect A-A' on Figure 1b) with a representation of climate change perturbations (changing recharge or P-ET, storm surge flooding, erosion, and sea-level rise). (b) HydroGeoSphere two-dimensional model domain and mesh with boundary conditions. The island domain dimensions changed for the erosion scenarios as described later.

volume numerical method to approximate solutions to the Richards (1931) equation for subsurface flow and the diffusion-wave approximation of the Saint-Venant (1871) equations for surface flow. For salt transport, only advection, diffusion, and dispersion transport processes were considered. Governing equations can be found in the Text S2 in Supporting Information S1 or in Aquanty (2015) and Therrien et al. (2010).

The conceptual model and mesh for the HydroGeoSphere 2D profile are shown in Figure 2, and the location for the cross-shore model transect is shown in Figure 1b. This cross-shore profile was selected as it is approximately aligned with the geophysical measurements and the wellfield. The model domain extends 340 m offshore to the deepest point in the measured bathymetry and 1,290 m landward to the groundwater divide (highest groundwater elevation) based off of a 3D steady-state numerical model of the island developed using MODFLOW-2005 (Harbaugh, 2005) in FloPy (Bakker et al., 2016) with the sharp interface SWI2 (Salt Water Intrusion) package (Bakker et al., 2013) (see Text S3 and S4, Figure S1 in Supporting Information S1). This 3D model was not employed for the investigations of SWI due to climate change stressors as it cannot represent storm surge overtopping (Figure 2a). The offshore extent was selected after various iterations considering different model extents to ensure the seaward boundary condition location did not artificially control onshore aquifer dynamics.

The HydroGeoSphere domain was 1,630 m long and 117 m deep (Figure 2b) and contained 21,571 elements. Mesh spacing ranged from 0.5 to 10 m, with finer spacing at the wellfield, the coastal transition zone (see dense, black mesh in Figure 2b), and the left-most and upper boundaries. The mesh was established after a mesh refinement study to achieve a balance between spatial resolution and computational efficiency, as run times were typically several days. The freshwater flux was applied along the upper boundary from the shoreline to the inland groundwater divide (blue zone,  $x = 340$ –1,630 m, Figure 2b). Lennox Island is closer to a circular (radially symmetric) island than a “strip” (axially symmetric) island, but the 2D profile model (Figure 2b) in HydroGeoSphere

**Table 1**  
*Subsurface and Surface HydroGeoSphere Model Parameters*

Model parameters (units)	Value
Upper aquifer, saturated $K$ ( $\text{m s}^{-1}$ )	$8 \times 10^{-5}$
Lower aquifer, saturated $K$ ( $\text{m s}^{-1}$ )	$8 \times 10^{-6}$
Aquitard, saturated $K$ ( $\text{m s}^{-1}$ )	$10^{-8}$
Specific storage, $S_s$ ( $\text{m}^{-1}$ )	$10^{-5}$
Porosity, $n$	0.35
Alpha, $\alpha$ , ( $\text{m}^{-1}$ ) <sup>a</sup>	1.85
Beta, $\beta^1$ (–)	2.0
Pore connectivity, $l_p$ (–)	0.5
Residual water saturation, $S_{wr}$ (–)	0.01
Minimum relative permeability, $k_r$ (–)	$10^{-20}$
Subsurface longitudinal, transverse, vertical transv. dispersivity, $\alpha_L$ , $\alpha_T$ , $\alpha_{TV}$ (m)	1.0, 0.1, 0.1
Surface longitudinal, transverse, vertical transv. dispersivity, $\alpha_L$ , $\alpha_T$ , $\alpha_{TV}$ (m)	50.0–100, 10.0, 10.0
Subsurface tortuosity, $\tau$ (–)	1.0
Coupling length (m)	0.001–0.1
Coupling dispersivity (m)	5.0
Manning's roughness coefficient $x$ -direction, $y$ -direction, $n_x$ , $n_y$ ( $\text{m}^{-1/3} \text{s}$ )	$1 \times 10^{-6}$ , $1 \times 10^{-6}$
Rill storage height (m)	$1 \times 10^{-4}$
Obstruction storage height (m)	0.0

*Note.* Hydraulic conductivity ( $K$ ) values were calibrated, while other values are standard properties in HydroGeoSphere or for the geologic units in question. Model parameters and equations are further detailed in Text S2 in Supporting Information S1. <sup>a</sup> $\alpha$  and  $\beta$  are the van Genuchten fitting parameters for the soil water characteristic curve.

assumes axial symmetry rather than radial symmetry. Previous analytical solutions (Fetter, 1972) have shown that the same head distribution results for a transect from an island's center to its shoreline for a strip island as for a circular island if the recharge is halved in the case of the strip island. Accordingly, 50% of the recharge (precipitation minus potential evapotranspiration) value (50% of  $512 \text{ mm yr}^{-1}$ ) was applied to the model to yield the correct head distribution for the approximately circular Lennox Island.

A freshwater equivalent head (Aquanty, 2015) and seawater concentration was specified along the seafloor boundary (red zone, Figure 2b). No-flow boundary conditions (green, Figure 2b) were applied to the bottom, right side, and left side of the domain. The bottom boundary represents a low-permeability zone above which groundwater flow is horizontal, while the right boundary is the inland groundwater divide location based on the 3D modeling (Figure S1 in Supporting Information S1).

Calibration was manually conducted using results from nearby borehole logs, well data, and geophysical measurements to form parameters and output constraints. The main calibration parameters were hydraulic conductivity values in the aquifers and aquitard, while other parameters were based on default values in HydroGeoSphere or appropriate values for the geologic environment. Manual calibration was conducted as automated calibration would not be possible given the run time of each simulation. The upper aquifer hydraulic conductivity was varied to achieve model congruence with the hydraulic heads at the observation wells and the freshwater-saltwater interface location at the shore and wellfield. However, matching the modeled interface location to the geophysical data was the primary calibration focus as the inertial interface location can be a more robust calibration target in small-island settings than dynamic hydraulic heads (Pavlovskii et al., 2022). Van Genuchten (1980) soil water characteristic curve values for a sandstone determined by Manna et al. (2019) were used to parametrize the soil water retention for the upper aquifer. Parameters and results of the calibration runs are presented in Table 1 and Figures S2 and S3 of the Supporting Information S1.

The coupling length (Equation S6, Text S2, in Supporting Information S1), which links the surface and subsurface domain equations through the dual node approach (Park et al., 2009), was initially set to 0.01 m to maintain model

**Table 2**  
*Boundary Conditions Applied to Climate Change Scenarios*

Change	Model run ID	Description
N/A	Initial condition (IC)	Calibrated initial conditions as described in Section 2.3
Erosion runs	E25 L	Eroded coastline (domain shifted) after 25 years, 30 cm/year.
	E25U <sup>a</sup>	Eroded coastline after 25 years, 90 cm/year; or after 75 years, 30 cm/year
	E50 L	Eroded domain coastline after 50 years, 30 cm/year
	E50U	Eroded domain coastline after 50 years, 90 cm/year
	E75U	Eroded domain coastline after 75 years, 90 cm/year
	E100 L	Eroded domain coastline after 100 years, 30 cm/year
	E100U	Eroded domain coastline after 100 years, 90 cm/year
Changing recharge runs	R1 <sup>b</sup>	P-ET rate of 370 mm/yr applied to landside surface boundary (BC)
	R2 <sup>b</sup>	P-ET rate of 413 mm/yr applied to landside surface boundary
	R3 <sup>b</sup>	P-ET rate of 556 mm/yr applied to landside surface boundary
Sea-level rise runs	SLR1	SLR applied to ocean surface node BC; 70 cm SLR by 2099, 7.7 mm/yr
	SLR2	SLR applied to ocean surface node BC; 90 cm SLR by 2099, 10 mm/yr
	SLR3	SLR applied to ocean surf. Node BC; 110 cm SLR by 2099, 12.2 mm/yr
Storm surge runs	S1	1.08 m surge applied to ocean surface node BC for 24-hr period
	S2	1.48 m surge applied to ocean surface node BC for 24-hr period
	S3	2.05 m surge applied to ocean surface node BC for 24-hr period
	S4	4.1 m surge applied to ocean surface node BC for 24-hr period
Combo run	C1	Eroded domain shoreline @ 100 years (90 cm/yr rate), P-ET is 370 mm/yr

<sup>a</sup>Eroded shoreline after 25 years at 90 cm yr<sup>-1</sup> has the same position as after 75 years at 30 cm yr<sup>-1</sup>. <sup>b</sup>P-ET rates were later halved when applied to the model as described in the text.

stability, but was later reduced to 0.001 m once steady-state conditions were achieved to run the climate change scenarios (Guimond & Michael, 2020; Paldor & Michael, 2021). The combined impact scenario described later had a coupling length of 0.1 m to maintain stability. Four pumping wells were included as sinks in the modeling domain, and the details on implementing the extraction rates can be found in Text S3 in Supporting Information S1. The model represents quasi-steady-state conditions. Therefore, the impacts of tides and waves on the coastal groundwater (LeRoux et al., 2021; Robinson et al., 2007), which are somewhat limited at the site given the lower tidal range and wave energy, were not accounted for. Initial conditions for the transient simulations (detailed below) were obtained by running the model until heads at observation locations stabilized and the freshwater zone thickness reached equilibrium.

## 2.4. Climate Change Scenarios

Table 2 provides an overview of the simulated climate change scenarios, including coastal erosion as a direct climate change impact. These different stressors were applied to the model by altering boundary conditions and/or boundary locations as described below. Impacts for the different stressors were compared by assessing new “post-stress” steady-state conditions (interface locations, freshwater volumes, and heads). While results were variable among runs, steady-state conditions were typically achieved around 1,000 years.

### 2.4.1. Changing Island Morphology (Erosion) Scenarios

Erosion rates at the southern shore of Lennox Island generally range between 0 and 30 cm yr<sup>-1</sup> (PEI, 2021). However, some areas have higher erosion rates (>90 cm yr<sup>-1</sup>, PEI, 2021), and coastlines are expected to experience more change as sea levels rise and storm surge frequencies and intensities increase. Therefore both 30 and 90 cm yr<sup>-1</sup> erosion rates were used to alter the island geometry and investigate steady-state hydraulic head and salinity distributions with truncated domains that represent 25, 50, 75, and 100 years of erosion. As the numerical model cannot easily accommodate a continuously adjusting boundary condition location due to gradual erosion (*i.e.*, shoreline

interface migration), we adjusted the model domain and assigned new shoreline boundary locations after a period of assumed constant erosion. For example, 90 cm/yr for 100 years resulted in a shoreline boundary location that was shifted 90 m inland. Once the shoreline position was adjusted by a distance equal to the erosion rate (30 cm yr<sup>-1</sup> and 90 cm yr<sup>-1</sup>) times the erosion timeline (25, 50, 75, and 100 years), the new model with a truncated domain (see Figure S4 in Supporting Information S1 for adjusted domains) was run to steady state to simulate the new freshwater volumes (runs E25 L to E100U, Table 2). A total of seven erosion scenarios were simulated, since 90 cm yr<sup>-1</sup> over 25 years is the same as 30 cm yr<sup>-1</sup> over 75 years. The erosion was assumed to occur as a landward moving vertical face, similar to erosion patterns during hurricanes on Prince Edward Island (e.g., Mulligan et al., 2023).

#### 2.4.2. Changing Recharge Scenarios

Monthly climate projections for Lennox Island were obtained from ClimataData.ca (Cannon et al., 2016; PCIC, 2022; Vincent et al., 2015) between 2071 and 2100. These data are based on CMIP5 projections under Representative Concentration Pathways (RCP) 2.6, 4.5, and 8.5. Median and upper values for daily minimum and maximum air temperatures and precipitation rates were obtained for the range of RCP4.5 and 8.5 scenarios from different climate models. Minimum and maximum daily air temperatures were used to calculate projected upper and median evapotranspiration rates for RCP4.5 and 8.5 using the FAO (2009) calculator. Recharge (precipitation minus evapotranspiration) values were obtained for each scenario, and if values were similar to the default recharge value, they were disregarded.

The resultant recharge change scenarios R1, R2, and R3 (Table 2) represent values of 370 (RCP 4.5 median), 413 (RCP 8.5 median), and 556 mm yr<sup>-1</sup> (RCP 4.5 or 8.5 upper), respectively. These are higher (556 mm yr<sup>-1</sup>) and lower (413 and 370 mm yr<sup>-1</sup>) recharge rates compared to the default value (512 mm yr<sup>-1</sup>), which is in line with previous research in Atlantic Canada that noted challenges in projecting the direction of groundwater recharge changes, let alone the magnitude (Kurylyk & MacQuarrie, 2013). As previously described, these recharge rates were all reduced by 50% in HydroGeoSphere to produce the heads in a radially symmetric aquifer (Fetter, 1972). These changing recharge simulations (Table 2) were run for 1,000 years to achieve a new steady-state freshwater distribution. For all simulations in this study, the freshwater volume was calculated by summing the porewater volumes for elements with concentrations less than 1,000 mg L<sup>-1</sup>.

#### 2.4.3. Sea-Level Rise Scenarios

SLR projections were obtained from James et al. (2021) based on IPCC AR5 modeling and the NAD83v70VG national crustal velocity model (Robin et al., 2020) between 2010 and 2099. The SLR scenarios considered in this study (SLR1, SLR2, and SLR3, Table 2) were respectively based on the 95th percentile (upper) projections for northern Prince Edward Island for RCP 2.6, 4.5, and 8.5 scenarios (Table 2). For the SLR simulations, the specified head boundary (Equation 1) was continuously increased at the respective SLR rate for 90 years (2010–2099) and was then run to steady state by maintaining the 2099 specified head value until the freshwater volume equilibrated.

#### 2.4.4. Storm Surge Scenarios

Surges were modeled in HydroGeoSphere by increasing the water depth at the ocean boundary condition by the respective surge level for the storm duration. Post-tropical Storm Dorian made landfall in Prince Edward Island in 2019 for approximately 24 hr (Avila et al., 2020; PEI, 2020), and was an extreme event in terms of both precipitation and maximum coastal water elevation. High-water levels (surges) of 1.05, 1.48, and 2.05 m above mean sea level were inferred based on water marks at three locations on Lennox Island (Jardine et al., 2021). These values were used for storm surge scenarios S1, S2, and S3 (Table 2) respectively. To help generalize the findings beyond this field site that has lower surges than some other locations worldwide, a fourth scenario, S4, represents a higher surge of 4.1 m (2 × S3) to consider the impacts of a storm that inundates a significant extent of the island. The coastal flooding extent associated with these surges is shown on Figure 1b. The 4.1 m surge extends further inland, including close to the model landward boundary condition from the northeast direction (A-A' transect, Figure 1b). However, the inundated area remains downgradient of the wellfield transect, allowing us to retain our no-flow, no-transport boundary condition on the landward side of the model transect.

To represent these surge conditions, the water depth at the ocean boundary condition (Figure 2b) was increased linearly to the respective surge level over 24 hr based on the timing of the peak surge and recession during Hurricane Dorian (Avila et al., 2020), before returning to mean sea level. After the surge, the model was run for 10 years. The 10-year mark was chosen because past studies have reported that aquifers reached potable conditions

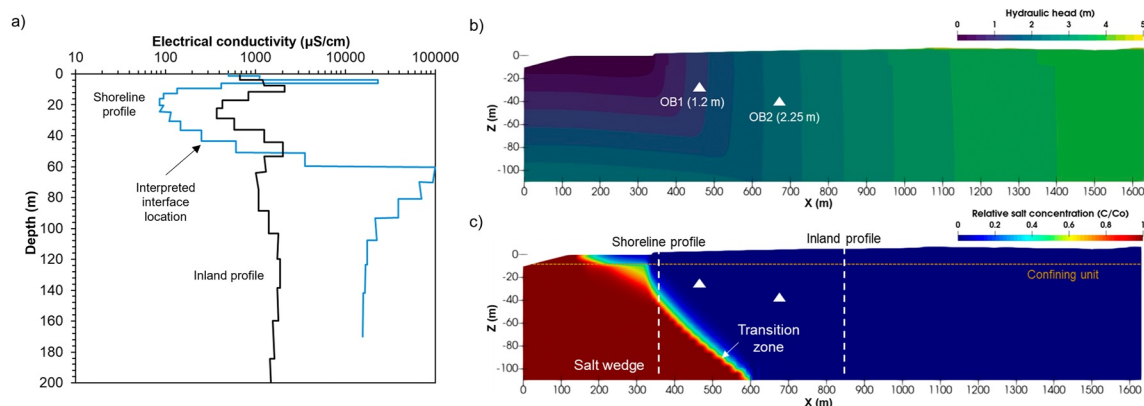


**Figure 3.** (a) Porewater electrical conductivity profiles from the bulk resistivity WalkTEM measurements (Figure 1b) at each location and converted using Archie's Law. (b) Modeled hydraulic head distribution for the present-day, steady-state initial conditions (run IC, Table 2). (c) Modeled relative salinity distribution for the same run as in panel (a) with the WalkTEM profile locations noted by vertical, dashed white lines (Figure 1b & panel (a)).

within about 10 years of a storm event (Anderson & Lauer, 2008; Yang et al., 2013). Importantly, recovery times that are longer than surge recurrence times may result in an accumulated salinization effect (Paldor et al., 2022). However, for the studied site and for small islands in general, it is likely that full recovery is reached on shorter time scales and therefore we neglected the effect of recurring storms. This also allowed us to isolate the impact of a given surge height and test variable magnitudes, which is the aim of the present study.

#### 2.4.5. Combined Reduced Recharge and High Erosion Scenario

Climate perturbations occur in tandem, and accordingly a combined impact scenario (run C1, Table 2) with a reduced domain representing 100 years of  $90 \text{ cm yr}^{-1}$  erosion and the lowest recharge was run to steady-state conditions. There are many other combinations of climate perturbations that could be considered, but we focused on one run with the two stressors (erosion and recharge reduction) that individually resulted in the most SWI for this site as discussed later (Sections 3.2 and 3.3).

### 3. Results

#### 3.1. Model Calibration and Initial Conditions for a Stable Climate

Prior to running simulations, we collected and interpreted field data to aid in model calibration. Figure 3a shows the resulting electrical conductivity profiles for the two WalkTEM station locations (Figure 1b), and Figure 3c shows these locations superimposed on the model domain. At the shoreline, the freshwater zone is approximately 43 m thick. This lens thickness at the shoreline is indicative of freshwater flux and confined aquifer conditions that resist the inland movement of the wedge. At the inland survey location, the WalkTEM survey indicates that the freshwater zone is at least 100 m deep as this is the depth of confidence from the geophysical inversion. These were the only locations we were able to collect measurements from without significant electromagnetic interference.

The hydraulic head and relative salt concentration distributions for the calibrated, steady-state model run (initial conditions, Table 2) that served as the initial conditions for subsequent climate change scenarios are shown in Figure 3. Simulated hydraulic heads at OB1 and OB2 are 1.20 and 2.25 m above sea level (model datum), respectively (Figure 3b), which results in a hydraulic gradient of approximately 0.005 between the two wells. While these were not our primary calibration target, the values are in reasonable agreement with the observed average values of 1.44 and 1.83 m. The simulated freshwater zone at the shoreline is approximately 35 m thick, and the 1,000 mg/L isoconcentration line of the saltwater wedge toe reaches  $x = 645 \text{ m}$ , which is 305 m inland from the pre-erosion shoreline located at 340 m (Figure 3c). At the inland geophysical measurement location (Figure 3a), the modeled freshwater-saltwater interface was at a depth of approximately 170 m (Figure 3c). In general, exactly matching both the observed hydraulic gradient between the monitoring wells and the shoreline interface depth proved to be challenging, and we focused more on calibrating to the shoreline interface depth (Pavolvskii et al., 2022). The freshwater volume for initial conditions, based on the  $1,000 \text{ mg L}^{-1}$  threshold for freshwater and a 1-m thickness in the alongshore dimension, was  $45,863 \text{ m}^3$ . For the initial condition, the

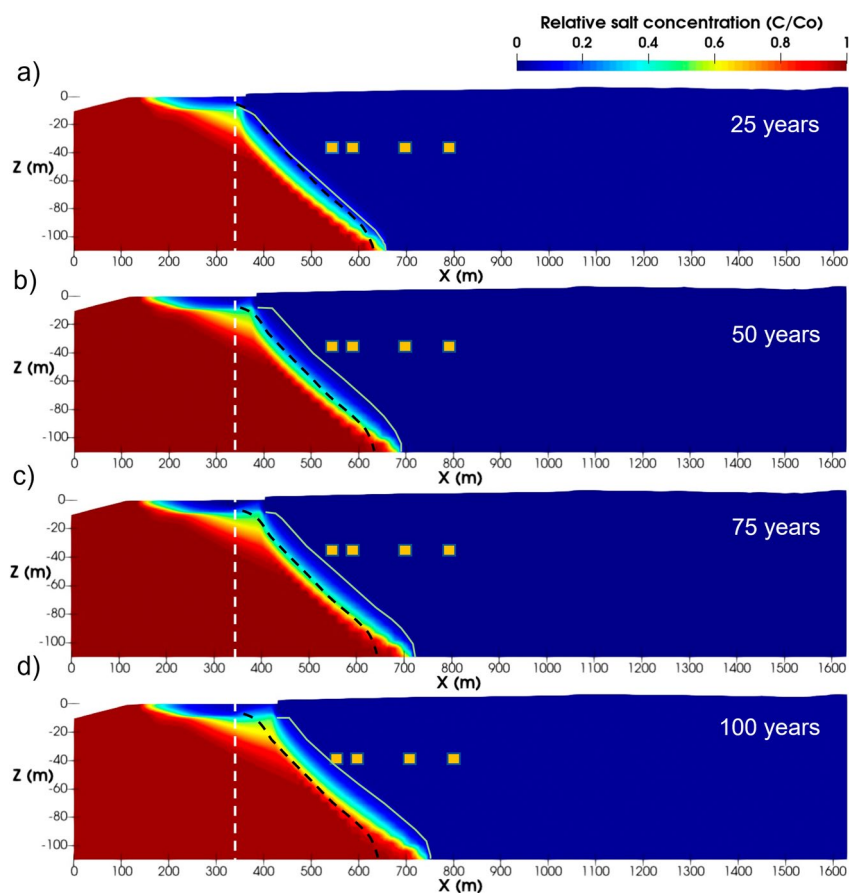


**Figure 4.** Steady-state salinity distributions for the higher erosion runs after 25, 50, 75, and 100 years of erosion: (a) E25U, (b) E50U, (c) E75U, and (d) E100U (see Table 2). The white dashed vertical line indicates the initial shoreline position, the black dashed line indicates the initial interface (1,000 mg/L isoconcentration) position, and the light gray line indicates the resulting steady-state interface position after erosion (1,000 mg/L isoconcentration). Yellow squares represent pumping wells.

water at the locations of the pumping wells was fresh. The calibrated hydraulic conductivity parameters are in Table 1. The climate change simulation runs described in the following sections were compared to these initial present-day results as summarized in Figure 3 and Table S2 (Supporting Information S1).

### 3.2. Impacts of Erosion

Steady-state salinity distributions for the high-erosion runs (runs E25U, E50U, E75U, and E100U, Table 2) are shown in Figure 4, and freshwater volume, heads, and interface locations for these runs are summarized in Figure 5. Simulated results for the lower erosion rate are presented in Figure S5 in Supporting Information S1. As the coastline was moved further inland due to erosion, hydraulic heads decreased and the saltwater wedge moved further inland (Figure 5). Hydraulic heads ranged from 0.53 to 1.12 m for OB1 and 1.75–2.25 m for OB2, as more of the shoreline was eroded. The saltwater wedge toe moved 10–110 m inland relative to the initial condition run for the different erosion scenarios (Figure 5 and Table S2 in Supporting Information S1) as the magnitude of shoreline erosion increased.

As expected, the freshwater volume decreased due to erosion as the shoreline was moved further inland (Figure 5a). Freshwater volumes ranged from 45,803 to 41,909 m<sup>3</sup> (up to 8.6% decrease from the initial condition run, Table 2) among all erosion scenarios, and also decreased approximately linearly with the increased length of eroded coastline (Figure 5a). Erosion scenario E100U had the most pronounced effects on hydraulic heads, freshwater volume, and saltwater wedge position, as it was also associated with the most pronounced erosion (Figures 5a and 5b). The erosion scenarios at 75 and 100 years led to salinization of the pumping well closest to the shoreline. The maximum concentration at the wellfield was 1,400 mg/L under a 100-year erosion scenario (90 cm yr<sup>-1</sup>), which is over five

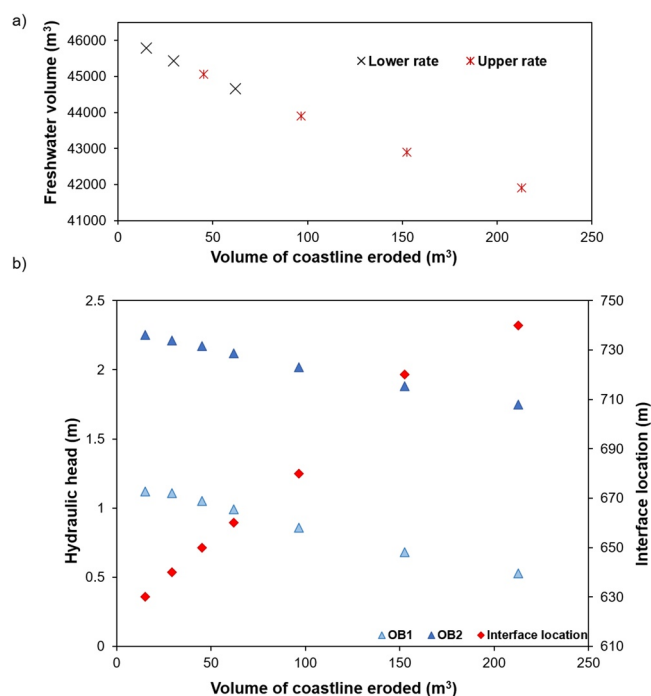


**Figure 5.** (a) Steady-state freshwater volume versus volume of eroded coastline for each erosion scenario (see Table 2 runs E25 L to E100 L for lower erosion rates and E25U to E100U for upper erosion rates), and (b) hydraulic heads for OB1 and OB2 and interface location at the wedge toe (red diamonds, with the value indicating the  $x$  position at the base of the domain, see Figure 4) for each erosion scenario.

times the maximum acceptable concentration (250 mg/L) for drinking water in Canada (Health Canada, 2020).

### 3.3. Impact of Changing Recharge

The resulting steady-state (1,000-year simulations) salt concentration distribution and saltwater wedge positions for the three changing recharge scenarios are shown in Figure 6a, and freshwater volume and hydraulic head evolution are shown in Figure S6 in Supporting Information S1. For run R1 (Table 2), decreasing the recharge value to 370 mm yr<sup>-1</sup> (originally 512 mm/year) resulted in hydraulic heads in OB1 and OB2 decreasing to 0.90 and 1.74 m, respectively (Figure S6 in Supporting Information S1). The saltwater wedge moved inland relative to the location for the initial condition run by approximately 170 m (Figure 6a), which salinized the well closest to the shore (560 mg/L). The freshwater volume in the domain decreased by 8% (Table S2 in Supporting Information S1).

Changing the recharge rate to 413 mm yr<sup>-1</sup> (run R2) also resulted in decreased hydraulic heads in the observation wells. OB1 and OB2 heads decreased to 0.98 and 1.89 m, respectively. The saltwater wedge toe moved 110 m landward (Figure 6a), and the steady-state freshwater volume decreased 5.2%. For R3 (increased recharge scenario), hydraulic heads at OB1 and OB2 increased to 1.29 and 2.41 m, respectively, the saltwater wedge toe moved seaward by 25 m (Figure 6a), and the freshwater volume increased by 1.6%.

### 3.4. Impact of Sea-Level Rise

The hydraulic head and freshwater volume changes for the SLR runs are shown in Figure S7 in Supporting Information S1, and the relative salt distribution and saltwater wedge positions for all three SLR scenarios at steady state (i.e., after 1,000 years of simulation time) are shown in Figure 6b. For

the run with 0.7-m of SLR (run SLR1) by 2100 and then with constant boundary conditions assigned until steady-state was achieved, the heads at OB1 and OB2 increased to 1.77 and 2.87 m, respectively (Figure S7 in Supporting Information S1). The saltwater wedge toe moved inland from the initial condition (Table 2) location by 35 m (Figure 6b), and the freshwater volume was decreased by 2.7% (Table S2 in Supporting Information S1). Under the SLR2 scenario, the 0.9-m SLR caused hydraulic heads in OB1 and OB2 to rise to 1.97 and 3.07 m, respectively. The saltwater wedge moved inland by 40 m, and the steady-state freshwater volume dropped by 2.7%. For the SLR3 scenario, the 1.1-m SLR caused heads to rise to 2.14 and 3.22 m in OB1 and OB2, respectively, the wedge moved 55 m inland, and the freshwater volume decreased by 3.5%. None of the three SLR scenarios resulted in salinization of the pumping wells (Figure 6b). At 100 years, the saltwater wedge position was at similar locations ( $x \approx 650$  m) under all three scenarios, indicating a lag between flow and saltwater wedge re-equilibration. However, by 1,000 years the three SLR scenarios produced different new steady-state results as summarized in Table S2 in Supporting Information S1.

### 3.5. Impacts of Storm Surge Overtopping

For the storm surge runs (S1–S4, Table 2), the respective observation well hydraulic head changes are shown in Figure S8 in Supporting Information S1. During the entirety of each simulation, the 24-hr storm event did not have a significant impact on the saltwater wedge, and no saltwater plumes developed in the upper aquifer. Given the similar results among runs, only the run S4 results are shown (Figure 7). The lack of salinization is explained briefly by the fact that most of the land surface on the modeled transect is above these storm surge heights (for runs S1–S3), and thus the surges only propagated short distances along the shoreline. For the 4.1 m storm surge (run S4), the surge did penetrate further inland as shown in the surge map (Figure 1b), but only negligible changes to the groundwater salinity occurred, and those were limited to the shallow aquifer (e.g., Figures 7e and 7f).

The relative resilience of the aquifer to salinization from storm surges is postulated to be due to the relatively small flooded area in the modeled transect (Figure 1b), as well as the vadose zone properties and hydraulic conductivity

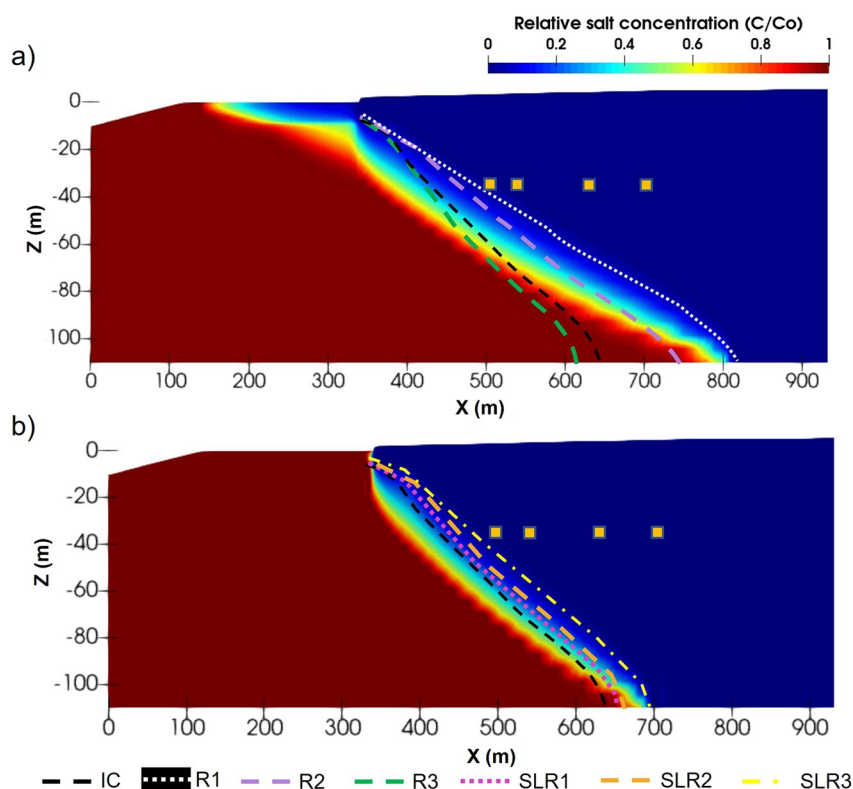


**Figure 6.** (a) Salinity distribution at steady state (domain truncated at  $x = 900$  m) for the changing recharge runs (Table 2). Interface positions (the 1,000 mg/L isocontour) are shown for model run R1 (white dotted line), R2 (purple dashed line), R3 (green dashed line, increased recharge), and initial conditions (black dashed line). (b) Normalized salinity distribution at steady-state (colors) and interface locations for the initial conditions (black line, Table 2) and sea-level rise runs SLR1 (pink dotted line), SLR2 (orange dashed line), and SLR3 (yellow dotted dash line).

of the upper aquifer that limited infiltration and facilitated rapid flushing of infiltrated water. Under each storm surge scenario, the hydraulic heads reached their maximum levels during the surge event and then re-equilibrated (Figure S8 in Supporting Information S1). For runs S1, S2, and S3, the freshwater volume decreased by only 0.007% during the storm surge, with insignificant differences among scenarios. The freshwater volume returned to its original value within 170 days after the storm event for runs S1 to S3. Even under run S4, the freshwater volume only decreased 0.013% from initial conditions, but it took much longer (16 years) to return to the initial freshwater volume. The salinity distribution was only affected for the shallow bathymetric portion of the model domain, while the aquifer zone pumped for groundwater supply was not impacted (Figure 7).

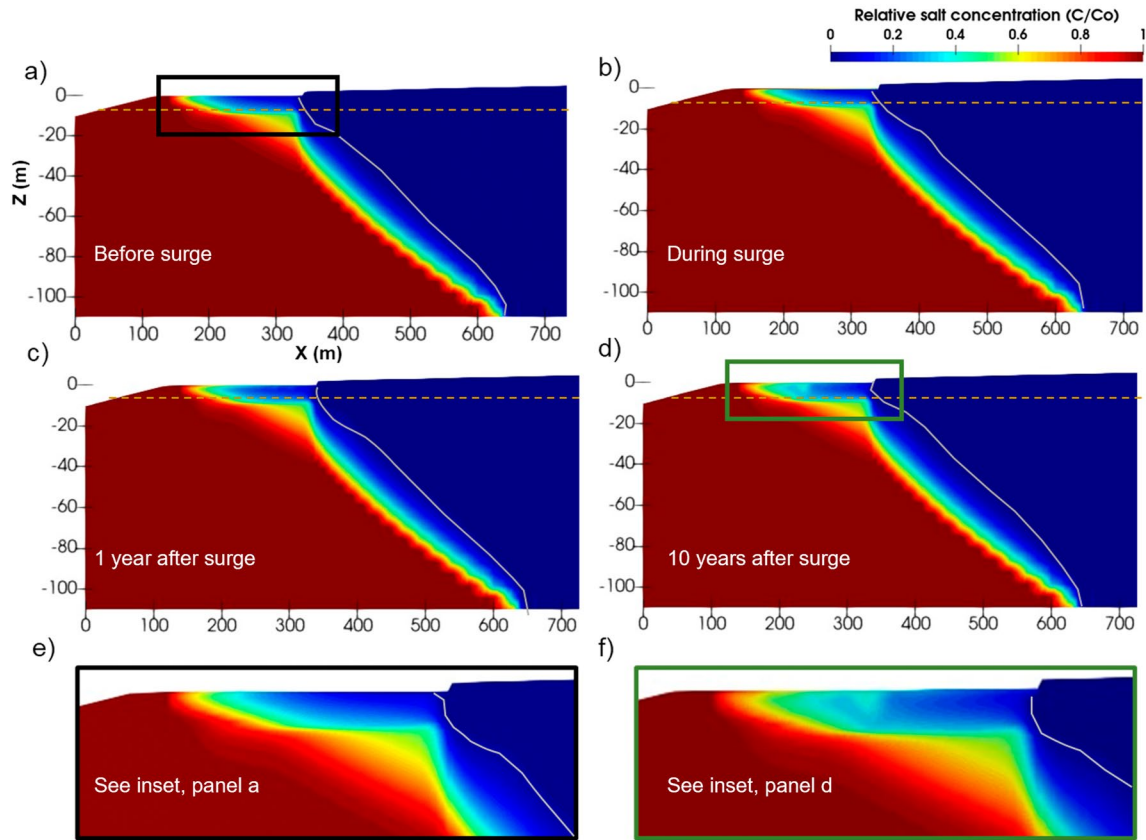
### 3.6. Impacts of the Combined Scenario (Erosion and Recharge Reduction)

Combining the impacts of reduced recharge and an eroded coastline (run C1, Table 2) had the most significant impacts on the aquifer based on changes in hydraulic head, freshwater volume, and salinity (Figure 8). Hydraulic heads at OB1 and OB2 decreased to 0.43 and 1.33 m, respectively. The saltwater wedge toe moved inland by 295 m, and the freshwater volume in the domain was decreased by 16%. The movement of the interface inland caused the salinity to increase to 11,200 mg/L at the first pumping well, and 6,195 mg/L at the second pumping well, which are both well above the 250 mg/L Health Canada (2020) drinking water standard.

## 4. Discussion

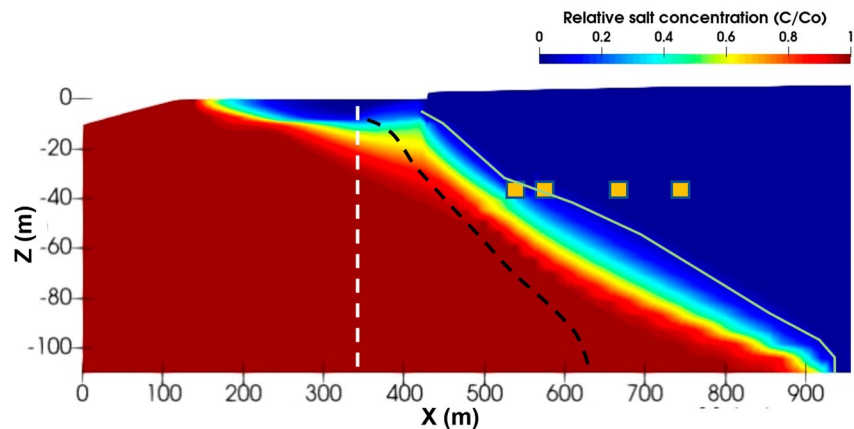
### 4.1. Erosion Impacts

Figure 9 shows a comparison of freshwater volumes and the saltwater wedge position with respect to the pumping wells for each model scenario (Table 2). Coastline erosion significantly impacted the freshwater-saltwater interface position (Figures 4 and 5) due to moving the saltwater boundary condition closer to the island center



**Figure 7.** Salinity distribution for surge run S4 (Table 2): (a) before, (b) during, (c) 1 year after, and (d) 10 years after with saline plumes only forming in the shallow portion of the ocean boundary ( $x = 117\text{--}340\text{ m}$ ). Panels (e) and (f) show a zoom-in of the shoreline for panels (a) and (d), respectively. The light gray lines indicate the  $1,000\text{ mg L}^{-1}$  isoconcentration line for each scenario (a–d). Longitudinal dispersivity was increased to 100 m in the surface domain for this simulation for numerical reasons. The horizontal, brown dashed line in a–d indicates the confining unit.

combined with the overall decrease in land area available for recharge (Chesnaux et al., 2021; Fetter, 1972). However, although there was an overall decrease in hydraulic heads throughout the aquifer system, the hydraulic gradient increased between observation wells OB1 and OB2. This may be attributed to the method in which erosion was simulated. With increased erosion, the vertical shoreline boundary dimension was increased, likely



**Figure 8.** Steady-state salinity distribution for the combined scenario (run C1, Table 2). The white vertical dashed line indicates initial shoreline position, the black dashed line indicates initial wedge position ( $1,000\text{ mg L}^{-1}$  contour), and the light gray line indicates the new steady-state wedge position ( $1,000\text{ mg L}^{-1}$  contour).

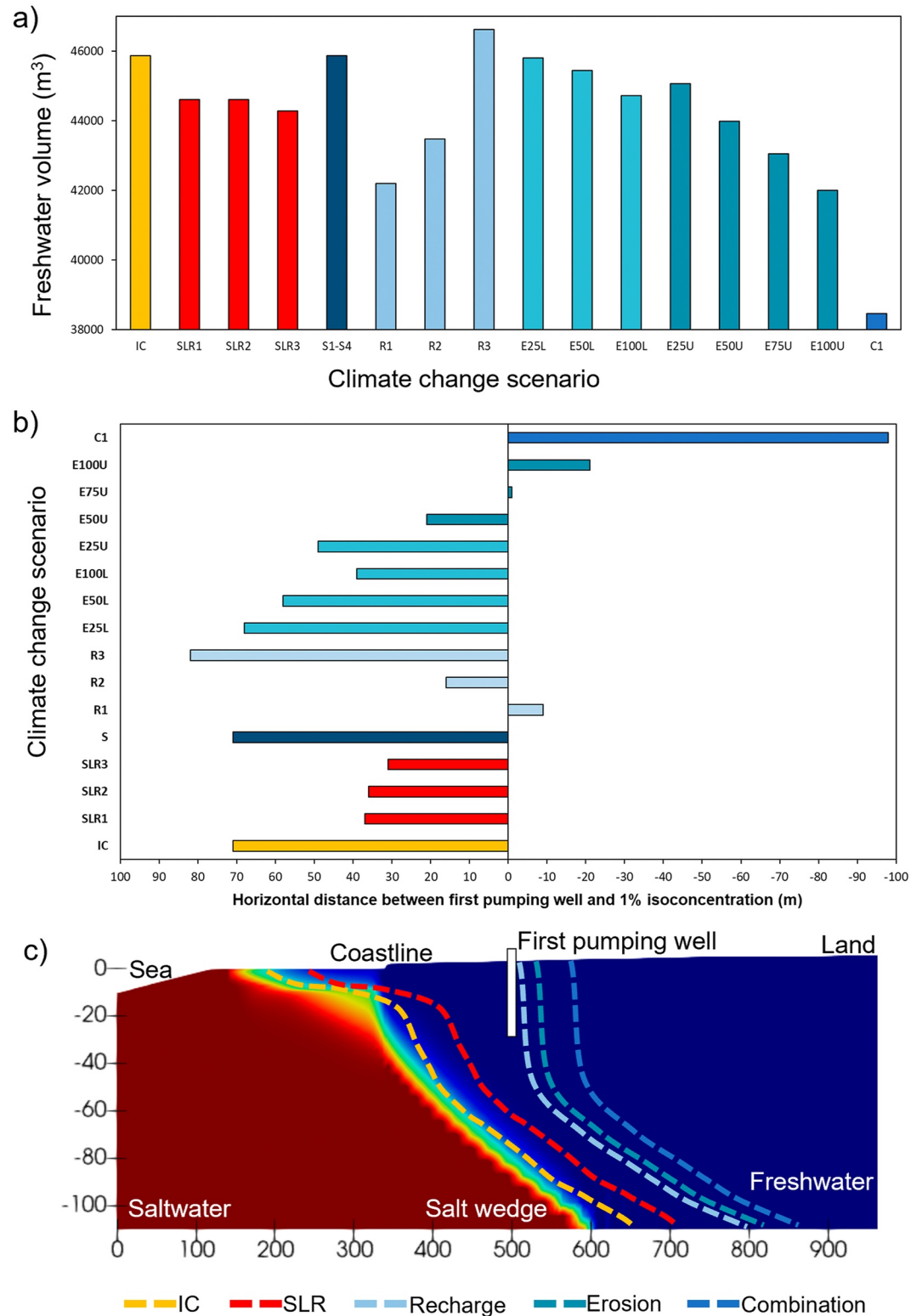


**Figure 9.** (a) Freshwater volumes, (b) horizontal distances between the first pumping well and the 1% isoconcentration line (an approximation of the drinking water threshold) at the same elevation as the well screen for all simulations in this study (Table 2), with colors indicating the grouping of perturbation types (e.g., red = sea-level rise, light blue = changing recharge), and (c) visual representation of wedge locations relative to the first pumping well (as shown in b). Negative values in panel (b) represent a wedge position that is further inland than the first pumping well (i.e., when the well was salinized to a value over the 1% concentration threshold).

increasing exfiltration, and decreasing hydraulic heads at shoreline locations. Much of Prince Edward Island's north shore was converted to steeper vertical faces, similar to how erosion was represented in the model, following the pronounced coastal erosion that occurred during Hurricane Fiona in September 2022 (e.g., Mulligan et al., 2023).

Compared with the reduced recharge scenarios, coastal erosion did not result in as large of an impact on freshwater volumes and saltwater wedge positions until later times. Also, the transition zone widened as more erosion occurred, which resulted in the first pumping well exceeding 1% salinity (Figure 9), with two scenarios resulting in concentrations well above the Canadian drinking water standard. Although the saltwater wedge location was not as sensitive to erosion as it was to recharge reductions, there are still significant long-term implications for freshwater availability due to erosion alone. For example, water managers often rely solely on hydroclimatic prediction in planning the development of future water resources. This study suggests that geomorphological predictions should be factored into the assessments, as fast-eroding areas along the coastline will likely experience faster inland salinization. These findings highlighting the role of coastal erosion in shrinking freshwater zones in island aquifers are in conceptual agreement with the work of Schneider and Kruse (2006) and Lemieux et al. (2015) on sandy, barrier islands, and are related to (but opposite) recent studies showing how sand accretion or nourishment on barrier islands can lead to the development of larger freshwater lenses (Holt et al., 2019; Huizer et al., 2018; Röper et al., 2013). Our findings highlight that bedrock coastlines, which are generally less morphodynamic than sandy barrier islands, can still experience erosion rates that are a significant contributor to SWI.

#### 4.2. Recharge Impacts

When the climate change perturbations were considered in isolation, reducing the recharge (run R1, Figure 6a) resulted in the largest shifts in the saltwater wedge (up to 170 m). This finding generally comports with the results from White and Falkland (2010) and Briggs et al. (2021) who found that recharge changes due to droughts or decadal climate oscillations rendered certain small-island aquifers unusable due to lens thinning. These findings are also in general agreement with previous studies that found that SWI driven by changes in recharge on islands or along marine continental coastlines is often greater than the extent of SWI driven by other stressors like SLR (Carretero et al., 2013; Chui & Terry, 2013; Ketabchi et al., 2016). These results emphasize that small-island groundwater vulnerability can be driven by atmospheric climate change as well as the marine climate change drivers discussed in the following sections.

#### 4.3. Sea-Level Rise Impacts

The SLR scenarios (Figure 6b) demonstrate that the magnitude of increased sea level during the 90-year period is important, with the effect of land-surface inundation being particularly important. The SLR1 and SLR2 runs yielded similar freshwater volumes, whereas SLR3 resulted in a lower freshwater volume as a tipping point was reached (Figure S7 in Supporting Information S1). Under the SLR1 and SLR2 scenarios, very little of the island inundates given the steep coast. After a certain limit is reached (i.e., the sea level under SLR3), the freshwater volume decreases significantly as a much larger portion of the shore is inundated. This suggests that an aquifer's response to SLR is not always proportional to the perturbation but may also be characterized by threshold response behavior (Webb & Howard, 2011), in this case due to the SLR rate relative to the coastal land surface elevation. Scenario SLR3 also resulted in the largest increase in hydraulic heads in the unconfined aquifer, which increased exfiltration to the surface domain. Similar to the findings of Watson et al. (2010) and Morgan et al. (2015), hydraulic heads re-equilibrated relatively fast, at approximately 100 years (i.e., 10 years after sea level stopped rising), whereas the more inertial saltwater wedge (Pavolvskii et al., 2022) only established a new steady-state position after approximately 500 years.

In contrast with the findings of prior numerical modeling studies and studies with analytical solutions for confined aquifers subject to SLR (Shi et al., 2018; Werner et al., 2013), the modeling results in this study showed a shift in the saltwater wedge toe position after SLR (Figure 6b), even with the presence of a confining layer. This is due to upward flow from the confined (leaky) aquifer into the unconfined aquifer as the sea level rose. The resulting rise in hydraulic heads in the confined aquifer did not match the SLR magnitude as in previous confined-aquifer modeling studies (e.g., Chang et al., 2011). This may be because the confining layer for previous studies has

often been placed along the top of the domain, which would not allow for upward flow from the confined aquifer. In contrast, in the present study, the confining unit was up to 15 m below ground surface and thus the system functioned as a topography-limited aquifer. Also, in the present study, the confining layer thickness is small relative to the size of the domain (0.6 m), and the hydraulic conductivity value assigned to the aquitard was not low enough to fully confine the lower aquifer, resulting in more SWI than in studies of more fully confined aquifers. This is important to consider in future studies of confined systems, since the hydrogeological configuration presented here may be more representative of certain natural systems, and the difference in the salinization dynamics may be substantial, according to our findings.

#### 4.4. Storm Surge Impacts

Storm surges had only a small impact on the hydraulic heads and an insignificant impact on the salinity distribution (Figure 7, Figure S8 in Supporting Information S1). The surge heights for model runs S1, S2, and S3 were not sufficient to inundate much of the modeled land surface due to the steep topography at the shoreline edge (Figure S9 in Supporting Information S1). This prevented any saline plumes (Post & Houben, 2017) from forming in the unconfined aquifer or migrating to deeper in the subsurface. Under run S4, although there was land-surface flooding, hydraulic heads in the upper aquifer increased enough to fully saturate the subsurface close to the shore. This resulted in significant exfiltration at the ground surface close to the shore. The combined impacts of erosion and storm surge were not addressed in this study since erosion was herein considered as a vertical cliff migrating inland, and thus the extent of surge-driven flooding was independent of erosion.

The storm surge scenarios differ from those in earlier studies for several reasons. Firstly, the surge height in this study was small. For example, Anderson and Lauer (2008) used a surge height of 3 m in a lower elevation setting than Lennox Island, Yang et al. (2013) used a surge height of 8.5 m, and Liu and Tokunaga (2019) used a surge level of 15 m. The storm surges in these previous studies were for typhoons and tsunamis, while the present study considered smaller but typical surges experienced for post-tropical storms in Prince Edward Island (Jardine et al., 2021; Mulligan et al., 2023). Also, the capacity for the aquifer to infiltrate coastal floodwater was lower in the present study than in other studies. For example, the upper aquifer hydraulic conductivity was almost two orders of magnitude lower than the hydraulic conductivity used by Yang et al. (2013) and Paldor and Michael (2021), reducing the infiltration occurring during a storm event (Yang et al., 2015). It is also important to note that the simulated storm surges caused significant inundation on Lennox Island, even if they had minimal impact in the modeled higher elevation transect that contained the wells (Figure 1b). We chose to focus our simulations on the pumped regions of the aquifer rather than in low-lying regions of Lennox Island; however, if wells were located elsewhere on the island, they could be extremely vulnerable to surges. Thus, the findings for this study related to the general resilience of the wellfield to storm surge flooding and vertical SWI do not necessarily extend to elsewhere on Lennox Island or to other low-lying islands worldwide (Oppenheimer et al., 2019) that have previously been shown to be vulnerable to vertical SWI following coastal flooding due to lower elevations, higher surges, or higher infiltration capacity (e.g., Cantelon et al., 2023; Storlazzi et al., 2018; Tajima et al., 2023).

#### 4.5. Combined Impacts (Changing Recharge and Erosion)

The paired climate perturbation run (C1, Table 2) with erosion and reduced recharge combined caused saltwater wedge migration that extended 125 m past any of the isolated runs (Figure 9c). These results strongly indicate that risks posed to fresh groundwater resources should not be considered in isolation. Atmospheric, oceanic, hydrologic, and morphologic changes act together, and these superimposed forcings may collectively further stress coastal aquifers. In this study, we only considered one paired run in which the dominant stressors were combined; future studies could investigate different combinations of stressors for field sites where oceanic and atmospheric projections, erosion susceptibility, and groundwater pumping conditions differ from those in the present study.

#### 4.6. Implications for Other Coastal Aquifers Experiencing Climate Change

This study reveals the relative *resilience* of the Lennox Island aquifer to SLR and storm surges and the relative *vulnerability* to changing recharge and erosion. However, the ranking of climate change threats may differ substantially for other coastal aquifers based on the hydrogeological conditions, coastal hydro- and morpho-dynamics, relative SLR rates, and potential recharge changes. For example, the insensitivity of the Lennox Island aquifer

to coastal storms arises in part from the relatively high ratio of land surface elevation to surge height for the modeled transect. As noted in Section 4.4, other studies for sites with different hydrodynamic and topographic conditions have considered much higher surges and/or lower elevations and shown surges to be important for SWI (e.g., Anderson & Lauer, 2008; LeRoux et al., 2023; Paldor & Michael, 2021). Also, waves and wave runup were not considered in this study as Lennox Island is in a protected bay that does not experience very large waves (Dolan, 2022). However, these dynamics may be important at other sites for raising water elevations beyond surge heights and overtopping engineered coastal barriers or natural berms and pooling seawater inland. Such dynamics could be considered by linking groundwater models with hydrodynamic models that represent more complex wave dynamics (Elsayed & Oumeraci, 2018; Storlazzi et al., 2018). Also, the relative insensitivity of the Lennox Island aquifer to storm surge is due in part to the low-permeability confining unit which impeded the downward migration of saltwater. The hydraulic conductivity for this unit (Table 1) is much lower than values used to model sandy barrier islands experiencing surge-driven flooding and lower than values used when modeling atoll island aquifers (e.g., Briggs et al., 2021).

The impacts of SLR on SWI dynamics depends strongly on whether the aquifer is recharge-limited or topography-limited (Michael et al., 2013), with the former conditions, which characterize the upper aquifer of Lennox Island, being less vulnerable. Additionally, the confining unit and pressurized deeper groundwater conditions contribute to the lower sensitivity of the Lennox Island aquifer to SLR. Sandy coastlines host shallow aquifers that function more as homogeneous, unconfined units that are more vulnerable to SLR than Lennox Island's aquifer. Also, the relative sensitivity of an island or coastal aquifer to changing recharge would differ along the global coastline as some coastal areas have historic trends or future projections that generally indicate increased precipitation (e.g., Curtis, 2019). Depending on the coincident changes in evapotranspiration, potential increases in recharge arising from increased precipitation could help combat SWI due to SLR (e.g., Threndyle et al., 2022).

Finally, this study points to the potential of coastal erosion as a major driver of SWI, which has not been considered in past large-scale analyses of future SWI (e.g., Ferguson & Gleeson, 2012). Coastal erosion is generally a global problem; however, some sections of the global coastline are experiencing accretion, with the global surface area of coastal erosion approximately twice that of coastal accretion (Mentaschi et al., 2018). Islands and continental coastlines undergoing natural or anthropogenic sediment deposition may experience a growth in the freshwater aquifer volumes that could partially offset erosion-driven SWI in other locations (Holt et al., 2019; Huizer et al., 2018; Röper et al., 2013). Sandy coasts, which make up 31% of the ice-free global shoreline, are particularly morphodynamic (Luijendijk et al., 2018), and thus past studies of erosion-driven SWI have focused on sandy islands (e.g., Schneider & Kruse, 2006; Lemieux et al., 2015). Results from the present study further reveal that erodible, consolidated coastlines may also experience erosion rates that are high enough to drive pronounced SWI. Collectively, these differences highlight the value of site-based research to understand how drivers of SWI vary across systems with differing geologic, hydrologic, and oceanic conditions, and what factors should be considered in management of fragile island freshwater resources.

## 5. Conclusions

We used results from field data and a coupled, integrated surface-subsurface model of water flow and transport to investigate the potential for SWI in a small-island, confined aquifer. We considered aquifer salinization in response to erosion, changing recharge, SLR, and storm surge overtopping. This is the first modeling study to consider the impacts of erosion on SWI into aquifers along islands or continental coastlines that are not sandy and thus less morphodynamic, and the first to consider erosion in an integrated surface-subsurface hydrologic model. Previous modeling studies of island aquifers have generally considered homogeneous or atoll island aquifers rather than the layered, confined bedrock (fractured sandstone) aquifer that was considered in the present study. Such confined island aquifers are common worldwide. Results of the model simulations show that the aquifer was most sensitive to changing recharge and erosion. These climate change stressors resulted in the largest reductions in freshwater volume and hydraulic head, and the largest inland shift of the freshwater-saltwater interface. For example, the interface at the bottom of the domain moved 110 and 170 m inland for the scenarios representing the highest erosion and greatest recharge reduction, respectively. When these scenarios were considered in combination, the wedge moved ~300 m inland and salinized the wellfield.

Sea-level rise also caused a shift in the saltwater wedge (55 m at 110 m depth) as the lower aquifer was not sufficiently confined to prevent saltwater wedge movement. Storm surges had little impact on the freshwater volume due to the limited spatial extent of surface inundation in the modeled transect during the storm events.

This allowed for hydraulic heads to re-equilibrate quickly and for any minimal salinization to be rapidly flushed. Under higher storm surges, the heads in the upper aquifer increased significantly, resulting in a large amount of exfiltration that limited downward migration of saltwater plumes.

While the study findings were based on a specific site in Atlantic Canada, our findings provide critical insight into freshwater insecurity on other small islands worldwide, particularly those with layered aquifer systems. Importantly, the model findings highlight risks, such as erosion, that island water managers should consider when developing climate change adaptation strategies focused on freshwater sustainability. Our model results show that climate change stressors on small-island aquifers can produce more deleterious impacts when considered in tandem (e.g., simultaneous erosion and reduced recharge). Given that our inland boundary condition represents a terrestrial groundwater divide rather than any distinctive island characteristic, our results are also applicable to confined aquifers along continental coastlines. Thus, findings emphasize the importance of considering how rapidly eroding marine coastlines can trigger SWI into critical coastal aquifers, especially when occurring in combination with changing ocean and atmospheric conditions. Model results reveal that the relative threats to freshwater resources in island aquifers depend strongly on the local hydrodynamic, geologic, and climatic conditions, and thus results for other islands may differ substantially from those in this study. Accordingly, these results point to the need for more paired field and modeling hydrogeological investigations for different coastal aquifer settings to develop a holistic framework for water resource managers conducting short-term and long-term island groundwater vulnerability assessments. Such vulnerability assessments could inform climate change adaptation solutions such as nature-based solutions to attenuate coastal flooding or managed aquifer recharge to increase hydraulic heads and interface depth and to accelerate flushing of salinized aquifers.

### Data Availability Statement

WalkTEM resistivity profiles for the inland and shoreline locations (Figure 3a) and model input files (\*.grok, \*.mprops, and \*.oprops) for the initial condition run (Table 2) are archived in Stanic (2024), which is available at: <https://doi.org/10.5683/SP3/ZAAY3M>. Observation well data were not released for public distribution other than figures.

### Acknowledgments

The project was funded through the Canada Research Chairs program, a MEOPAR Early-Career Award, and an NSERC Discovery Grant (RGPIN-2018-05420) to B. Kurylyk. S. Stanic was supported through the NSERC CREATE ASPIRE program. A. Paldor and H. Michael were supported by US NSF Grant OIA1757353.

This manuscript was reviewed and approved by the Luney/Mi'kmaq Confederacy of PEI Research Ethics Board. We thank the Lennox Island First Nation (LIFN) for allowing us to conduct this research on their land, the Mi'kmaq Confederacy of PEI and the LIFN for logistically supporting this project, and Mr. Travis Dymont for providing technical support related to observation well data and pumping operations on Lennox Island. We also thank Aquanty for their support during the modelling process. Igor Pavlovskii is thanked for developing a 3D MODFLOW-SWI2 model to ascertain the location of the groundwater divide on Lennox Island (supporting information). We thank the Associate Editor and two anonymous reviewers for helpful comments that improved the clarity of this paper.

### References

- Afzaal, H., Farooque, A. A., Abbas, F., Acharya, B., & Esau, T. (2020). Computation of evapotranspiration with artificial intelligence for precision water resource management. *Applied Sciences*, 10(5), 1621. <https://doi.org/10.3390/app10051621>
- Anderson, W. P., Jr., & Lauer, R. M. (2008). The role of overwash in the evolution of mixing zone morphology within barrier islands. *Hydrogeology Journal*, 16(8), 1483–1495. <https://doi.org/10.1007/s10040-008-0340-z>
- Aquanty Inc. (2015). *HydroGeoSphere user manual* (p. 435). Waterloo.
- Armon, J. W., & McCann, S. B. (1979). Morphology and landward sediment transfer in a transgressive barrier island system, southern Gulf of St. Lawrence, Canada. *Marine Geology*, 31(3–4), 333–344. [https://doi.org/10.1016/0025-3227\(79\)90041-0](https://doi.org/10.1016/0025-3227(79)90041-0)
- Ataie-Ashtiani, B., Werner, A. D., Simmons, C. T., Morgan, L. K., & Lu, C. (2013). How important is the impact of land-surface inundation on seawater intrusion caused by sea-level rise? *Hydrogeology Journal*, 21(7), 1673–1677. <https://doi.org/10.1007/s10040-013-1021-0>
- Avila, L. A., Stewart, S. R., Berg, R., & Hagen, A. B. (2020). National hurricane center part of the National Ocean and Atmospheric Administration (NOAA) tropical cyclone report. Hurricane Dorian (AL052019). [https://www.nhc.noaa.gov/data/tcr/AL052019\\_Dorian.pdf](https://www.nhc.noaa.gov/data/tcr/AL052019_Dorian.pdf)
- Bakker, M., Post, V., Langevin, C. D., Hughes, J. D., White, J. T., Starn, J. J., & Fienen, M. N. (2016). Scripting MODFLOW model development using Python and FloPy. *Ground Water*, 54(5), 733–739. <https://doi.org/10.1111/gwat.12413>
- Bakker, M., Schaars, F., Hughes, J. D., Langevin, C. D., & Dausman, A. M. (2013). Documentation of the seawater intrusion (SWI2) package for MODFLOW. In *U.S. Geological Survey Techniques and Methods, book 6*. Chapter A46, p. 47. Retrieved from <https://pubs.usgs.gov/tm/6a46/>
- Barlow, P. M., & Reichard, E. G. (2010). Saltwater intrusion in coastal regions of North America. *Hydrogeology Journal*, 18(1), 247–260. <https://doi.org/10.1007/s10040-009-0514-3>
- Bilskie, M. V., Hagen, S. C., Medeiros, S. C., & Passeri, D. L. (2014). Dynamics of sea level rise and coastal flooding on a changing landscape. *Geophysical Research Letters*, 41(3), 927–934. <https://doi.org/10.1002/2013gl058759>
- Briggs, M. A., Cantelon, J. A., Kurylyk, B. L., Kulongoski, J. T., Mills, A., & Lane, J. W. (2021). Small atoll fresh groundwater lenses respond to a combination of natural climatic cycles and human modified geology. *Science of the Total Environment*, 756, 143838. <https://doi.org/10.1016/j.scitotenv.2020.143838>
- Cannon, A. J. (2016). Multivariate bias correction of climate model outputs: Matching marginal distributions and inter-variable dependence structure. *Journal of Climate*, 29(19), 7045–7064. <https://doi.org/10.1175/JCLI-D-15-0679>
- Cantelon, J. A., Guimond, J. A., Robinson, C. E., Michael, H. A., & Kurylyk, B. L. (2022). Vertical saltwater intrusion in coastal aquifers driven by episodic flooding: A review. *Water Resources Research*, 58(11), e2022WR032614. <https://doi.org/10.1029/2022WR032614>
- Cantelon, J. A., Robinson, C. E., & Kurylyk, B. L. (2023). Morphologic, atmospheric, and oceanic drivers cause multi-temporal saltwater intrusion on a remote, sand island. *Water Resources Research*, 59(10), e2023WR035820. <https://doi.org/10.1029/2023WR035820>
- Carr, P. A. (1969). Salt-water intrusion in Prince Edward Island. *Canadian Journal of Earth Sciences*, 6(1), 63–74. <https://doi.org/10.1139/e69-007>
- Carretero, S., Rapaglia, J., Bokuniewicz, H., & Kruse, E. (2013). Impact of sea-level rise on saltwater intrusion length into the coastal aquifer, Partido de La Costa, Argentina. *Continental Shelf Research*, 61–62, 62–70. <https://doi.org/10.1016/j.csr.2013.04.029>

- Chang, S. W., & Clement, T. P. (2012). Experimental and numerical investigation of saltwater intrusion dynamics in flux-controlled groundwater systems. *Water Resources Research*, 48(9). <https://doi.org/10.1029/2012wr012134>
- Chang, S. W., Clement, T. P., Simpson, M. J., & Lee, K.-K. (2011). Does sea-level rise have an impact on saltwater intrusion? *Advances in Water Resources*, 34(10), 1283–1291. <https://doi.org/10.1016/j.advwatres.2011.06.006>
- Chesneau, R., Marion, D., Boumaiza, L., Richard, S., & Walter, J. (2021). An analytical methodology to estimate the changes in fresh groundwater resources with sea-level rise and coastal erosion in strip-island unconfined aquifers: Illustration with Savary Island, Canada. *Hydrogeology Journal*, 29(3), 1355–1364. <https://doi.org/10.1007/s10040-020-02300-0>
- Chui, T. F. M., & Terry, J. P. (2013). Influence of sea-level rise on freshwater lenses of different atoll island sizes and lens resilience to storm-induced salinization. *Journal of Hydrology*, 502, 18–26. <https://doi.org/10.1016/j.jhydrol.2013.08.013>
- Curtis, S. (2019). Means and long-term trends of global coastal zone precipitation. *Scientific Reports*, 9(1), 5401. <https://doi.org/10.1038/s41598-019-41878-8>
- De St Venant, B. (1871). Théorie du mouvement non permanent des eaux, avec application aux crues des rivières et a l'introduction de marées dans leurs lits. *Comptes Rendus de l'Académie des Sciences*, 73, 147–154.
- De Jong, R., Qian, B., & Yang, J. Y. (2008). Modelling nitrogen leaching in Prince Edward Island under climate change scenarios. *Canadian Journal of Soil Science*, 88(1), 61–78. <https://doi.org/10.4141/cjss07032>
- Dolan, K. (2022). *Hydrodynamic forcing and erosion dynamics on two small islands off the north shore of Prince Edward island: A baseline assessment (Master's Thesis)*. Dalhousie University.
- ECCC. (2020a). Historical data, Harrington, Prince Edward Island. [Station ID 830P01; 2013–2017]. [https://climate.weather.gc.ca/climate\\_data/hourly\\_data\\_e.html?hlyRange=2004-03-25%7C2022-04-17&dlyRange=2000-07-01%7C2022-04-17&mlyRange=2000-07-01%7C2007-07-01&StationID=30308&Prov=PE&urlExtension=\\_e.html&searchType=stnProv&optLimit=specDate&StartYear=2013&EndYear=2017&selRowPerPage=25&Line=6&Month=1&Day=1&lstProvince=PE&timeframe=1&Year=2013](https://climate.weather.gc.ca/climate_data/hourly_data_e.html?hlyRange=2004-03-25%7C2022-04-17&dlyRange=2000-07-01%7C2022-04-17&mlyRange=2000-07-01%7C2007-07-01&StationID=30308&Prov=PE&urlExtension=_e.html&searchType=stnProv&optLimit=specDate&StartYear=2013&EndYear=2017&selRowPerPage=25&Line=6&Month=1&Day=1&lstProvince=PE&timeframe=1&Year=2013)
- ECCC. (2020b). Historical data, Summerside, Prince Edward Island. [Station ID 8300596]. [https://climate.weather.gc.ca/climate\\_data/daily\\_data\\_e.html?hlyRange=1994-02-01%7C2022-04-17&dlyRange=1999-07-19%7C2022-04-17&mlyRange=2004-01-01%7C2007-07-01&StationID=10800&Prov=PE&urlExtension=\\_e.html&searchType=stnProv&optLimit=specDate&StartYear=2013&EndYear=2017&selRowPerPage=25&Line=15&Month=1&Day=1&lstProvince=PE&timeframe=2&Year=2013](https://climate.weather.gc.ca/climate_data/daily_data_e.html?hlyRange=1994-02-01%7C2022-04-17&dlyRange=1999-07-19%7C2022-04-17&mlyRange=2004-01-01%7C2007-07-01&StationID=10800&Prov=PE&urlExtension=_e.html&searchType=stnProv&optLimit=specDate&StartYear=2013&EndYear=2017&selRowPerPage=25&Line=15&Month=1&Day=1&lstProvince=PE&timeframe=2&Year=2013)
- Elsayed, S. M., & Oumeraci, H. (2018). Modelling and mitigation of storm-induced saltwater intrusion: Improvement of the resilience of coastal aquifers against marine floods by subsurface drainage. *Environmental Modelling & Software*, 100, 252–277. <https://doi.org/10.1016/j.envsoft.2017.11.030>
- Falkland, A. C. (1993). Hydrology and water management on small tropical islands. In *Hydrology of warm humid regions (Proceedings of the Yokohama Symposium, July 1993)*. IAHS Publication no. 216.
- Ferguson, G., & Gleeson, T. (2012). Vulnerability of coastal aquifers to groundwater use and climate change. *Nature Climate Change*, 2(5), 342–345. <https://doi.org/10.1038/nclimate1413>
- Fetter, C. W. (1972). Position of the saline water interface beneath oceanic islands. *Water Resources Research*, 8(5), 1307–1315. <https://doi.org/10.1029/wr008i005p01307>
- Food and Agriculture Organization of the United Nations ETo Calculator. (2009). Retrieved from <https://www.fao.org/land-water/databases-and-software/eto-calculator/en/>
- Glover, P. W. J. (2016). Archie's law – A reappraisal. *Hydrology and Earth System Sciences*, 7(4), 1157–1169. <https://doi.org/10.5194/se-7-1157-2016>
- Gohar, A. A., Cashman, A., & Ward, F. A. (2019). Managing food and water security in small island states: New evidence from economic modelling of climate stressed groundwater resources. *Journal of Hydrology*, 569, 239–251. <https://doi.org/10.1016/j.jhydrol.2018.12.008>
- Greenan, B. J. W., James, T. S., Loder, J. W., Pepin, P., Azetsu-Scott, K., Ianson, D., et al. (2019). Changes in oceans surrounding Canada. In Bush & Lemmen (Eds.), *Canada's changing climate report* (pp. 343–423). Government of Canada. Chapter 7.
- Guimond, J. A., & Michael, H. A. (2020). Effects of marsh migration on flooding, saltwater intrusion, and crop yield in coastal agricultural land subject to storm surge inundation. *Water Resources Research*, 57(2). <https://doi.org/10.1029/2020wr028326>
- Harbaugh, A. W. (2005). MODFLOW-2005, the U.S. Geological Survey modular ground-water model—The ground-water flow process. *U.S. Geological Survey Techniques and Methods*, 6-A16.
- Health Canada. (2020). *Guidelines for Canadian Drinking Water Quality—Summary Table*. Water and Air Quality Bureau, Healthy Environments and Consumer Safety Branch. Health Canada.
- Hill, H. J., & Milburn, J. D. (1956). Effect of clay and water salinity on electrochemical behavior of reservoir rocks. *Transactions of the AIME*, 207(01), 65–72. <https://doi.org/10.2118/532-g>
- Holding, S., & Allen, D. M. (2015a). From days to decades: Numerical modelling of freshwater lens response to climate change stressors on small low-lying islands. *Hydrology and Earth System Sciences*, 19(2), 933–949. <https://doi.org/10.5194/hess-19-933-2015>
- Holding, S., & Allen, D. M. (2015b). Wave overwash impact on small islands: Generalised observations of freshwater lens response and recovery for multiple hydrogeological settings. *Journal of Hydrology*, 529, 1324–1335. <https://doi.org/10.1016/j.jhydrol.2015.08.052>
- Holding, S., Allen, D. M., Foster, S., Hsieh, A., Larocque, I., Klassen, J., & Van Pelt, S. C. (2016). Groundwater vulnerability on small islands. *Nature Climate Change*, 6(12), 1100–1103. <https://doi.org/10.1038/nclimate3128>
- Holt, T., Greskowiak, J., Seibert, S. L., & Massmann, G. (2019). Modeling the evolution of a freshwater lens under highly dynamic conditions on a currently developing barrier island. *Geofluids*, 2019, 9484657. <https://doi.org/10.1155/2019/9484657>
- Huizer, S., Radermacher, M., de Vries, S., Oude Essink, G. H. P., & Bierkens, F. P. (2018). Impact of coastal forcing and groundwater recharge on the growth of a freshwater lens in a mega-scale beach nourishment. *Hydrology and Earth System Sciences*, 22(2), 1065–1080. <https://doi.org/10.5194/hess-22-1065-2018>
- IPCC. (2021). In V. Masson-Delmotte, P. Zhai, A. Pirani, S. L. Connors, C. Péan, et al. (Eds.), *Climate change 2021: The physical science basis. Contribution of working group I to the sixth assessment report of the intergovernmental panel on climate change*. Cambridge University Press. <https://doi.org/10.1017/9781009157896>
- Jacques Whitford Environmental Limited. (2007). Comprehensive study report, water supply upgrade, Lennox island, Prince County, Prince Edward island. PWGSC Project No. 315883.
- James, T. S., Robin, C., Henton, J. A., & Craymer, M. (2021). Relative sea-level projections for Canada based on the IPCC fifth assessment report and the NAD83v70VG national crustal velocity model. *Geological Survey of Canada, Open File*, 8764. <https://doi.org/10.4095/327878>
- Jardine, D. E., Wang, X., & Fenech, A. L. (2021). Highwater mark collection after post tropical storm Dorian and implications for Prince Edward Island, Canada. *Water*, 13(22), 3201. <https://doi.org/10.3390/w13223201>
- Jiang, Y., & Somers, G. (2009). Modeling effects of nitrate from non-point sources on groundwater quality in an agricultural watershed in Prince Edward Island, Canada. *Hydrogeology Journal*, 17(3), 707–724. <https://doi.org/10.1007/s10040-008-0390-2>

- Jiang, Y., Somers, G., & Mutch, J. (2004). Application of numerical modeling to groundwater assessment and management in Prince Edward Island. In *Proceedings of the 57th Canadian Geotechnical Conference* (Vol. 57, pp. 2–9).
- Kang, H.-Y., Nielsen, P., & Hanslow, D. J. (1994). Watertable overheight due to wave runup on a sandy beach. In *Coastal Engineering 1994, Proceedings of the 24th International Conference on Coastal Engineering*. Kobe. <https://doi.org/10.1061/9780784400890.154>
- KarisAllen, J. J., Mohammed, A. M., Tamborski, J. J., Jamieson, R. C., Danieleescu, S., & Kurylyk, B. L. (2022). Present and future thermal regimes of intertidal groundwater springs in a threatened coastal ecosystem. *Hydrology and Earth System Sciences*, 26(18), 4721–4740. <https://doi.org/10.5194/hess-26-4721-2022>
- Ketabchi, H., Mahmoodzadeh, D., Ataie-Ashtiani, B., & Simmons, C. T. (2016). Sea-Level rise impacts on seawater intrusion in coastal aquifers: Review and integration. *Journal of Hydrology*, 535, 235–255. <https://doi.org/10.1016/j.jhydrol.2016.01.083>
- Ketabchi, H., Mahmoodzadeh, D., Ataie-Ashtiani, B., Werner, A. D., & Simmons, C. T. (2014). Sea-level rise impact on fresh groundwater lenses in two-layer small islands. *Hydrological Processes*, 28(24), 5938–5953. <https://doi.org/10.1002/hyp.10059>
- Kundzewicz, Z. W., Mata, L. J., Arnell, N. W., Doll, P., Kabat, P., Jimenez, B., et al. (2007). Freshwater resources and their management. In M. L. Parry, O. F. Canziani, J. P. Palutikof, P. J. van derLinden, & C. E. Hanson (Eds.), *Climate Change 2007: Impacts, Adaptation and Vulnerability. Contribution of Working Group II to the Fourth Assessment Report of the Intergovernmental Panel on Climate Change* (pp. 173–210). Cambridge University Press. ISBN 9780521880091.
- Kurylyk, B. L., & MacQuarrie, K. T. B. (2013). The uncertainty associated with estimating future groundwater recharge: A summary of recent research and an example from a small unconfined aquifer in a northern humid-continental climate. *Journal of Hydrology*, 492, 244–253. <https://doi.org/10.1016/j.jhydrol.2013.03.043>
- Lemieux, J.-M., Hassaoui, J., Molson, J., Therrien, R., Therrien, P., Chouteau, M., & Ouellet, M. (2015). Simulating the impact of climate change on the groundwater resources of the Magdalen Islands, Québec, Canada. *Journal of Hydrology: Regional Studies*, 3, 400–423. <https://doi.org/10.1016/j.ejrh.2015.02.011>
- LeRoux, N. K., Frey, S. K., Lapen, D. R., Guimond, J. A., & Kurylyk, B. L. (2023). Mega-tidal and surface flooding controls on coastal groundwater and saltwater intrusion within agricultural dikelands. *Water Resources Research*, 59(11), e2023WR035054. <https://doi.org/10.1029/2023WR035054>
- LeRoux, N. K., Kurylyk, B. L., Briggs, M. A., Irvine, D. J., Tamborski, J. J., & Bense, V. F. (2021). Using heat to trace vertical water fluxes in sediment experiencing concurrent tidal pumping and groundwater discharge. *Water Resources Research*, 57(2), e2020WR027904. <https://doi.org/10.1029/2020WR027904>
- Liu, J., & Tokunaga, T. (2019). Future risks of tsunami-induced seawater intrusion into unconfined coastal aquifers: Insights from numerical simulations at Nijijima island, Japan. *Water Resources Research*, 55(12), 10082–10104. <https://doi.org/10.1029/2019wr025386>
- Luijendijk, A., Hagenaars, G., Ranasinghe, R., Baart, F., Donchyts, G., & Aarninkhof, S. (2018). The state of the world's beaches. *Scientific Reports*, 8(1), 6641. <https://doi.org/10.1038/s41598-018-24630-6>
- MacDonald, K. (2014). Modeling present and future physical coastal vulnerability to climate change: North shore, Prince Edward island [Master's thesis, University of Waterloo]. *UWSpace*. <http://hdl.handle.net/10012/8482>
- Majeed, M. (2015). Examining the Effect of Visualization Tool Exposure on Local-level Stakeholder Perceptions on Climate Change Adaptation. [Master's thesis, University of Waterloo]. *UWSpace*. <http://hdl.handle.net/10012/9595>
- Manna, F., Murray, S., Abbey, D., Martin, P., Cherry, J., & Parker, B. (2019). Spatial and temporal variability of groundwater recharge in a sandstone aquifer in a semiarid region. *Hydrology and Earth System Sciences*, 23(4), 2187–2205. <https://doi.org/10.5194/hess-23-2187-2019>
- Mentaschi, L., Vousdoukas, M. I., Pekel, J.-F., Voukouvalas, E., & Freyn, L. (2018). Global long-term observations of coastal erosion and accretion. *Scientific Reports*, 8(1), 12876. <https://doi.org/10.1038/s41598-018-30904-w>
- Michael, H. A., Post, V. E. A., Wilson, A. M., & Werner, A. D. (2017). Science, society, and the coastal groundwater squeeze. *Water Resources Research*, 53(4), 2610–2617. <https://doi.org/10.1002/2017wr020851>
- Michael, H. A., Russoniello, C. J., & Byron, L. A. (2013). Global assessment of vulnerability to sea-level rise in topography-limited and recharge-limited coastal groundwater systems. *Water Resources Research*, 49(4), 2228–2240. <https://doi.org/10.1002/wrcr.20213>
- Morgan, L. K., Bakker, M., & Werner, A. D. (2015). Occurrence of seawater intrusion overshoot. *Water Resources Research*, 51(4), 1989–1999. <https://doi.org/10.1002/2014wr016329>
- Morgan, L. K., & Werner, A. D. (2014). Seawater intrusion vulnerability indicators for freshwater lenses in strip islands. *Journal of Hydrology*, 508, 322–327. <https://doi.org/10.1016/j.jhydrol.2013.11.002>
- Mulligan, R. P., Swatridge, L., Cantelon, J. A., Kurylyk, B. L., George, E., & Houser, C. (2023). Local and remote storm surge contributions to total water levels in the Gulf of St. Lawrence during Hurricane Fiona. *Journal of Geophysical Research: Oceans*, 128(8), e2023JC019910. <https://doi.org/10.1029/2023JC019910>
- NASA POWER. (2022). NASA prediction of worldwide energy resources (POWER) project. Retrieved from <https://power.larc.nasa.gov/> <https://power.larc.nasa.gov/>
- Nielsen, P., & Hanslow, D. J. (1991). Wave runup distributions on natural beaches. *Journal of Coastal Research*, 7(4), 1139–1152. <https://www.jstor.org/stable/4297933>
- Oppenheimer, M., Glavovic, B. C., Hinkel, J., van de Wal, R., Magnan, A. K., Abd-Elgawad, A., et al. (2019). IPCC special report on the ocean and cryosphere in a changing climate. In H.-O. Pörtner, D. C. Roberts, V. Masson-Delmotte, P. Zhai, M. Tignor, E. Poloczanska, et al. (Eds.), *Sea level rise and implications for low-lying islands, coasts and communities* (pp. 321–445). Cambridge University Press. <https://doi.org/10.1017/9781009157964.006>
- Paldor, A., Frederiks, R. S., & Michael, H. A. (2022). Dynamic steady state in coastal aquifers is driven by multi-scale cyclical processes, controlled by aquifer storativity. *Geophysical Research Letters*, 49(11), e2022GL098599. <https://doi.org/10.1029/2022GL098599>
- Paldor, A., & Michael, H. A. (2021). Storm surges cause simultaneous salinization and freshening of coastal aquifers, exacerbated by climate change. *Water Resources Research*, 57(5). <https://doi.org/10.1029/2020wr029213>
- Paldor, A., Shalev, E., Katz, O., & Aharonov, E. (2019). Dynamics of saltwater intrusion and submarine groundwater discharge in confined coastal aquifers: A case study in northern Israel. *Hydrogeology Journal*, 27(5), 1611–1625. <https://doi.org/10.1007/s10040-019-01958-5>
- Paradis, D., Vigneault, H., Lefebvre, R., Savard, M. M., Ballard, J.-M., & Qian, B. (2016). Groundwater nitrate concentration evolution under climate change and agricultural adaptation scenarios: Prince Edward Island, Canada. *Earth System Dynamics*, 7(1), 183–202. <https://doi.org/10.5194/esd-7-183-2016>
- Park, Y.-J., Sudicky, E. A., Panday, S., & Matanga, G. (2009). Implicit sub-time stepping for solving nonlinear equations of flow in an integrated surface-subsurface system. *Vadose Zone Journal*, 8(4), 825–836. <https://doi.org/10.2136/vzj2009.0013>
- Passeri, D. L., Hagen, S. C., Medeiros, S. C., Bilskie, M. V., Alizad, K., & Wang, D. (2015). The dynamic effects of sea level rise on low-gradient coastal landscapes: A review. *Earth's Future*, 3(6), 159–181. <https://doi.org/10.1002/2015ef000298>

- Pavlovskii, I., Jiang, Y., Danielescu, S., & Kurylyk, B. L. (2023). Influence of precipitation event magnitude on baseflow and coastal nitrate export for Prince Edward Island, Canada. *Hydrological Processes*, 37(5), e14892. <https://doi.org/10.1002/hyp.14892>
- Pavlovskii, I., Cantelon, J. A., & Kurylyk, B. L. (2022). Coastal groundwater model calibration using filtered and amplified hydraulic information retained in the freshwater-saltwater interface. *Hydrogeology Journal*, 30(5), 1551–1567. <https://doi.org/10.1007/s10040-022-02510-8>
- PCIC. (2022). Climate Data Canada – Collaboration of Pacific Climate Impacts Consortium, Ouranos Inc., Prairie Climate Centre, Environment and Climate Change Canada, Centre de Recherche Informatique de Montreal, and Habitat7. (2010). Climatedata.ca. Retrieved from <https://climatedata.ca>
- PEI. (2020). *Prince Edward Island after action review, post tropical storm Dorian*. Government of Prince Edward Island. Retrieved from [https://www.princeedwardisland.ca/sites/default/files/publications/final\\_calian\\_report\\_2020\\_1.pdf](https://www.princeedwardisland.ca/sites/default/files/publications/final_calian_report_2020_1.pdf)
- PEI. (2021). *Island information, interactive PEI maps*. Government of Prince Edward Island. Retrieved from <http://www.gov.pe.ca/maps/island-information.php3>
- Post, V. E. A., & Houben, G. J. (2017). Density-driven vertical transport of saltwater through the freshwater lens on the island of Baltrum (Germany) following the 1962 storm flood. *Journal of Hydrology*, 551, 689–702. <https://doi.org/10.1016/j.jhydrol.2017.02.007>
- Public Services and Procurement Canada. (2018). Lennox Island 2018 groundwater quality monitoring report.
- Richards, L. A. (1931). Capillary conduction of liquids through porous mediums. *Physics*, 1(5), 318–333. <https://doi.org/10.1063/1.1745010>
- Robin, C. M. I., Craymer, M., Ferland, R., James, T. S., Lapelle, E., Piraszewski, M., & Zhao, Y. (2020). NAD83v70VG: A new national crustal velocity model for Canada. Geomatics Canada, Open file 62. <https://publications.gc.ca/site/eng/9.901506/publication.html>
- Robins, N. S., & Lawrence, A. R. (2000). Some hydrogeological problems peculiar to various types of small islands. *Water and Environment Journal*, 14(5), 341–346. <https://doi.org/10.1111/j.1747-6593.2000.tb00271.x>
- Robinson, C., Li, L., & Prommer, H. (2007). Tide-induced recirculation across the aquifer-ocean interface. *Water Resources Research*, 43(7), W07428. <https://doi.org/10.1029/2006WR005679>
- Röper, T., Greskowiak, J., Freund, H., & Massmann, G. (2013). Freshwater lens formation below juvenile dunes on a barrier island (Spiekeroog, Northwest Germany). *Estuarine, Coastal and Shelf Science*, 121–122, 40–50. <https://doi.org/10.1016/j.ecss.2013.02.004>
- Schneider, J. C., & Kruse, S. E. (2003). A comparison of controls on freshwater lens morphology of small carbonate and siliciclastic islands: Examples from barrier islands in Florida, USA. *Journal of Hydrology*, 284(1–4), 253–269. <https://doi.org/10.1016/j.jhydrol.2003.08.002>
- Schneider, J. C., & Kruse, S. E. (2006). Assessing selected natural and anthropogenic impacts on freshwater lens morphology on small barrier Islands: Dog Island and St. George Island, Florida, USA. *Hydrogeology Journal*, 14(1–2), 131–145. <https://doi.org/10.1007/s10040-005-0442-9>
- Shi, Q., Lu, C., Ye, Y., Wu, J., Li, L., & Luo, J. (2018). Assessment of the impact of sea-level rise on steady-state seawater intrusion in a layered coastal aquifer. *Journal of Hydrology*, 563, 851–862. <https://doi.org/10.1016/j.jhydrol.2018.06.046>
- SPIA. (2020). Processing and inversion of ground-based TEM data. Retrieved from <https://hgg.au.dk/software/spia/>
- Stanic, S. (2024). Lennox Island field data and model inputs [Dataset]. Borealis. <https://doi.org/10.5683/SP3/ZA3V3M>
- Storlazzi, C. D., Gingerich, S. B., van Dongeren, A. P., Cheriton, O. M., Swarzenski, P. W., Quataert, E., et al. (2018). Most atolls will be uninhabitable by the mid-21st century because of sea-level rise exacerbating wave-driven flooding. *Science Advances*, 4(4), eaap9741. <https://doi.org/10.1126/sciadv.aap9741>
- Tackley, H. A., Kurylyk, B. L., Lake, C. B., Lapen, D. R., & van Proosdij, D. (2023). Impacts of repeated coastal flooding on soil and groundwater following managed dike realignment. *Science of the Total Environment*, 893, 164957. <https://doi.org/10.1016/j.scitotenv.2023.164957>
- Tajima, S., Brunner, P., Liu, J., Delottier, H., & Tokunaga, T. (2023). Groundwater flooding on atolls caused by storm surges: Effects of the dual-aquifer configuration. *Water Resources Research*, 59(10), e2023WR034762. <https://doi.org/10.1029/2023WR034762>
- Therrien, R., McLaren, R. G., Sudicky, E. A., & Panday, S. M. (2010). *HydroGeoSphere: A three-dimensional numerical model describing fully-integrated subsurface and surface flow and solute transport*. HydroGeoSphere Manual, Waterloo.
- Threndyle, R. E., Jamieson, R. C., Kennedy, G., Lake, C. B., & Kurylyk, B. L. (2022). Future inundation of coastal on-site wastewater treatment systems in a region with pronounced sea-level rise. *Journal of Hydrology*, 614(B), 128548. <https://doi.org/10.1016/j.jhydrol.2022.128548>
- Tribble, G. (2008). Ground water on tropical Pacific islands—Understanding a vital resource. *US Geological Survey Circular*, 1312, 35. <https://pubs.usgs.gov/circ/1312/>
- UNESCO-IHP & UNEP. (2016). *Transboundary Aquifers and Groundwater Systems of Small Island Developing States: Status and Trends, Summary for Policy Makers*. United Nations Environment Programme (UNEP). Retrieved from <https://unesdoc.unesco.org/ark:/48223/pf0000244912>
- Vacher, L. H. L., & Quinn, T. M. (1997). *Geology and hydrogeology of carbonate islands* (1st ed., p. 948). Elsevier Science.
- van de Poll, H. W. (1989). Lithostratigraphy of the Prince Edward Island red beds. *Atlantic Geology*, 25(1), 23–35. <https://doi.org/10.4138/1668>
- van der Kamp, G. (1981). Salt-water intrusion in a layered coastal aquifer at York Point, Prince Edward Island. In *National hydrology research institute paper 14, inland waters directorate series 121*. NHRI.
- van Genuchten, M. T. (1980). A closed-form equation for predicting the hydraulic conductivity of unsaturated soils. *Soil Science Society of America Journal*, 44(5), 892–898. <https://doi.org/10.2136/sssaj1980.03615995004400050002x>
- Vigneault, H., Paradis, D., Ballard, J. M., & Lefebvre, R. (2007). Numerical modelling of the evolution of groundwater nitrate concentrations under various Climate Change scenarios and agricultural practices for Prince Edward Island. Chapter 8. In M. M. Savard & G. Somers (Eds.), *In Consequences of climatic changes on contamination of drinking water by nitrate on Prince Edward Island*. Peer reviewed project report A881/A843. Natural Resources Canada, Climate Change Action Fund - Impacts & Adaptation, 29–39.
- Vincent, L. A., Zhang, X., Brown, R. D., Feng, Y., Mekis, E., Milewska, E. J., et al. (2015). Observed trends in Canada's climate and influence of low-frequency variability modes. *Journal of Climate*, 28(11), 4545–4560. <https://doi.org/10.1175/JCLI-D-14-00697.1>
- Vithanage, M., Engesgaard, P., Jensen, K. H., Illangasekare, T. H., & Obeyesekere, J. (2012). Laboratory investigations of the effects of geologic heterogeneity on groundwater salinization and flush-out times from a tsunami-like event. *Journal of Contaminant Hydrology*, 136–137, 10–24. <https://doi.org/10.1016/j.jconhyd.2012.05.001>
- Volker, R. E., Mariño, M. A., & Rolston, D. E. (1985). Transition zone width in ground water on ocean atolls. *Journal of Hydraulic Engineering*, 111(4), 659–676. [https://doi.org/10.1061/\(ASCE\)0733-9429\(1985\)111:4\(659\)](https://doi.org/10.1061/(ASCE)0733-9429(1985)111:4(659))
- Walther, M., Graf, T., Kolditz, O., Liedl, R., & Post, V. (2017). How significant is the slope of the sea-side boundary for modelling seawater intrusion in coastal aquifers? *Journal of Hydrology*, 551, 648–659. <https://doi.org/10.1016/j.jhydrol.2017.02.031>
- Watson, T. A., Werner, A. D., & Simmons, C. T. (2010). Transience of seawater intrusion in response to sea level rise. *Water Resources Research*, 46(12). <https://doi.org/10.1029/2010wr009564>
- Webb, M. D., & Howard, K. W. F. (2011). Modeling the transient response of saline intrusion to rising sea-levels. *Ground Water*, 49(4), 560–569. <https://doi.org/10.1111/j.1745-6584.2010.00758.x>

- Werner, A. D., Bakker, M., Post, V. E. A., Vandenbohede, A., Lu, C., Ataie-Ashtiani, B., et al. (2013). Seawater intrusion processes, investigation and management: Recent advances and future challenges. *Advances in Water Resources*, *51*, 3–26. <https://doi.org/10.1016/j.advwatres.2012.03.004>
- Werner, A. D., Sharp, H. K., Galvis, S. C., Post, V. E. A., & Sinclair, P. (2017). Hydrogeology and management of freshwater lenses on atoll islands: Review of current knowledge and research needs. *Journal of Hydrology*, *551*, 819–844. <https://doi.org/10.1016/j.jhydrol.2017.02.047>
- Werner, A. D., & Simmons, C. T. (2009). Impact of Sea-Level Rise on Sea Water Intrusion in Coastal Aquifers. *Ground Water*, *47*(2), 197–204. <https://doi.org/10.1111/j.1745-6584.2008.00535.x>
- White, I., & Falkland, T. (2010). Management of freshwater lenses on small Pacific islands. *Hydrogeology Journal*, *18*(1), 227–246. <https://doi.org/10.1007/s10040-009-0525-0>
- Winsauer, W. O., & Shearin, H. M. (1952). Resistivity of brine-saturated sands in relation to pore geometry. *AAPG Bulletin*, *36*. <https://doi.org/10.1306/3d9343f4-16b1-11d7-8645000102c1865d>
- World Population Review. (2023). How many islands are there in the world in 2023? Retrieved from <https://worldpopulationreview.com/geography/how-many-islands-are-there-in-the-world>
- Yang, J., Graf, T., Herold, M., & Ptak, T. (2013). Modelling the effects of tides and storm surges on coastal aquifers using a coupled surface–subsurface approach. *Journal of Contaminant Hydrology*, *149*, 61–75. <https://doi.org/10.1016/j.jconhyd.2013.03.002>
- Yang, J., Graf, T., & Ptak, T. (2015). Sea level rise and storm surge effects in a coastal heterogeneous aquifer: A 2D modelling study in northern Germany. *Grundwasser*, *20*(1), 39–51. <https://doi.org/10.1007/s00767-014-0279-z>
- Yu, X., Yang, J., Graf, T., Koneshloo, M., O'Neal, M. A., & Michael, H. A. (2016). Impact of topography on groundwater salinization due to ocean surge inundation. *Water Resources Research*, *52*(8), 5794–5812. <https://doi.org/10.1002/2016wr018814>
- Zebarth, B. J., Danielescu, S., Nyiraneza, J., Ryan, M. C., Jiang, Y., Grimmett, M., & Burton, D. L. (2015). Controls on nitrate loading and implications for BMPs under intensive potato production systems in Prince Edward Island, Canada. *Groundwater Monitoring & Remediation*, *35*(1), 30–42. <https://doi.org/10.1111/gwmmr.12088>
- Zhang, Y., Li, L., Erler, D. V., Santos, I., & Lockington, D. (2016). Effects of alongshore morphology on groundwater flow and solute transport in a nearshore aquifer. *Water Resources Research*, *52*(2), 990–1008. <https://doi.org/10.1002/2015wr017420>

## References From the Supporting Information

- Archie, G. E. (1942). The electrical resistivity log as an aid in determining some reservoir characteristics. *Transactions of the AIME*, *1*, 54–62.